eLife

Reviewed Preprint
v1 • January 5, 2026
Not revised

For correspondence:
federico.trigo@pedeciba.edu.uy

* Present address: Departamento de Señalización Neuronal y Glial, Instituto de Investigaciones Biológicas Clemente Estable, Montevideo, Uruguay.

Competing interests: No competing interests declared

Funding: See page 23

Reviewing editor: Jimena Berni, University of Sussex, United Kingdom

PKD2L1 channels segregated to the apical compartment are the exclusive dual-mode pH sensor in cerebrospinal fluid-contacting neurons

Magdalena Vitar[1,*], Daniel Prieto[1], Stavros Malas[2], Raúl E Russo[1], Federico F Trigo[1,*]

[1]Departamento de Neurofisiología Celular y Molecular, Instituto de Investigaciones Biológicas Clemente Estable, Montevideo, Uruguay • [2]The Cyprus Institute, Nicosia, Cyprus

eLife Assessment

This is an **important** study on the sensory roles of Cerebrospinal fluid-contacting neurons (CBF-cn) in mammals. The authors identify PKD2L1 as the predominant pH-sensing channel CBF-cn and show how the apical extension is used as an amplifier of chemical changes in the content of the Cerebrospinal fluid. The evidence is **solid** in experimental design but limited in mechanistic interpretation, as the electrophysiological analyses require re-evaluation.

https://doi.org/10.7554/eLife.109372.1.sa3

Abstract

Cerebrospinal fluid contacting neurons (CSFcNs) are GABAergic cells that surround the central canal (CC) of the spinal cord. Their soma is located sub-ependymally and they have a dendritic-like process that ends as a bulb (the so-called “apical process”; ApPr) inside the CC. It remains unclear how this unique anatomical organization, with the soma and the ApPr located in different extracellular environments, relates to their function as a multimodal sensor of cerebrospinal fluid (CSF) composition. One of the main physiological features of CSFcNs is a prominent spontaneous electrical activity mediated by PKD2L1 (or TRPP2) channels, a non-selective cation channel of the TRP family. PKD2L1 channels have a high single-channel conductance (around 200 pS) and can be modulated by protons and mechanical forces. In this work we investigate PKD2L1 channel sensitivity to pH and its effects on CSFcNs excitability. We demonstrate that PKD2L1 spontaneous activity generates not only phasic inward currents, but also a tonic current, both of which are modulated bidirectionally by pH with a high sensitivity around physiological values. By combining electrophysiology (direct recordings from intact and isolated ApPrs) with optical methods (laser-photolysis of protons) we further show that functional PKD2L1 channels are specifically localized in the ApPr. The spatial segregation of PKD2L1 channels, along with their biophysical properties (high single-channel conductance and pH sensitivity) and the ApPr’s unique membrane properties (very high input resistance) renders CSFcN excitability exquisitely sensitive to PKD2L1 modulation. Altogether, our findings illustrate how the ApPr’s properties are finely tuned to support its sensory role.

Introduction

Sensory information originates from the stimulation of specific receptors in different parts of the body. Beyond the five classic senses (touch, taste, smell, vision, and hearing), it has long been recognized that other sensory information—such as proprioception and visceral sensation—is fundamental for normal bodily function. Located at the interface between the spinal cord’s central canal (CC) and the spinal cord parenchyma, cerebrospinal fluid-contacting neurons (CSFcNs) are

part of a sensory system that provides information about the internal environment, specifically the composition of cerebrospinal fluid (CSF), and are thus considered part of the interoceptive system[1,2].

Sensory cells transduce sensory stimuli into electrical activity and typically have distinctive morphological specializations. CSFcNs are no exception, with their somas located in the subependymal layer from which a short, thick dendrite arises, ending in a bulbous structure located within the CC[3,4] known as the "apical process" (ApPr). The axon of CSFcNs, on the other hand, projects rostrally trough the ipsilateral ventral spinal cord, and contacts other CSFcNs and neurons of spinal central pattern generators, including motorneurons and premotor excitatory neurons[5–7]. By providing sensory information about CSF composition and the mechanical forces acting near the CC, CSFcNs participate in the control of posture and locomotion, both in lower vertebrates[1,5,8–10] and in rodents[6,7].

CSFcNs are established chemoreceptors. Huang et al. were the first to report that CSFcNs in the mouse spinal cord: i. express the PKD2L1 (or TRPP2) channel, a cation permeable channel of the TRP (Transient Receptor Potential) family that has a high Ca^{++} permeability[11]; ii. respond to acid with an increase in firing rate[12]. Subsequent studies examined the pH sensitivity of CSFcNs in the rat[3], lamprey[10,13] and mouse spinal cord[14,15]. These collective findings suggested that the response of CSFcNs to acidification depends on the activation of an acid sensing ion channel (ASIC), rapidly desensitizing inward current, and the response to alkalinization depends on the activation of PKD2L1 channels.

Despite previous work, the precise mechanisms and subcellular localization of the channels responsible for the pH response in CSFcNs remain unknown. This gap is partly due to two main factors. First, earlier investigations relied on bath application or pressure ejection of solutions with varying pH, which lack the spatial and temporal precision required to resolve localized pH sensitivity in specific cellular compartments. Second, there are technical challenges associated with recording from a small neuronal compartment using electrophysiological approaches. Here, we overcome these technical barriers with a combination of whole-cell and outside-out recordings directly from the ApPr, along with laser photolysis of protons and immunohistochemistry. We reveal that PKD2L1 generates not only phasic but also a novel tonic current that critically shapes the membrane potential of CSFcNs. These currents exhibit high pH sensitivity near the physiological range. Importantly, we demonstrate that functional PKD2L1 channels are exclusively localized to the ApPr, whose high input resistance and pH sensitivity make it a highly specialized sensory hub for the integration of chemical signals.

Results

PKD2L1-mediated spontaneous activity in CSFcNs from Gata3^{eGFP} mice

In this work we used the Gata3^{eGFP}[16] transgenic mice, where CSFcNs express eGFP under a GATA3 regulatory element. GATA3 is a transcription factor expressed in the spinal cord both by CSFcNs[17] and V2b interneurons[16]. Figure 1A shows sagital (**Aa**) and transverse (**Ab**) slices of Gata3^{eGFP} animals where the typical morphology and location (around the CC) of CSFcNs can be readily appreciated. This, together with the fact that V2b interneurons are located well away from the CC, allows unambiguous identification of CSFcNs. As expected, GFP+ in the Gata3^{eGFP} mice express the PKD2L1 channel showing they are indeedCSFcNs (Figure 1Ac and **d**). We first characterised the basal electrophysiological activity of CSFcNs from Gata3^{eGFP} mice in voltage-clamp, as these neurons in the Gata3^{eGFP} transgenic have not yet been characterized. CSFcNs were recorded with a KGluconate-based intracellular solution (IS) at near physiological temperature (34 ± 1 °C) with the whole-cell configuration of the patch-clamp technique from either the soma or the ApPr; neurons were clamped at -60 mV. In these conditions, spontaneous single-channel events were recorded, confirming previous results (in mice[14,15], lamprey[10] and zebrafish[18]). Figure 1Ba shows a 1 sec period of such a recording. The dotted horizontal green lines indicate 3 levels of

channel activity (c = closed; o1 = 1 channel open; o2 = 2 channels open). Figure 1Bb shows the corresponding histogram, where the 3 peaks that define the 3 levels of channel activity are shown with arrowheads. From the analysis, the probability of each state (pc, po1 and po2) was calculated. In this example, the single channel current recorded at -60 mV holding potential was -17.5 pA, and po1 was 0.12. From the spontaneous activity of different CSFcNs recorded either from the ApPr or from the soma, we measured an average single channel current amplitude of -15.9 ± 1.8 pA (Figure 1Bc, n = 38, with minimal and maximal values of -12.1 and -19.3, respectively) and a highly variable average probability for 1 channel being open, po1, of 0.08 ± 0.08 at -60 mV (Figure 1Bd, n = 38, with minimal and maximal values of 0.0065 and 0.29, respectively). No difference was found for these two values between ApPr and somatic recordings (p = 0.06 for the single channel current and p = 0.53 for po1), and the results were pooled together (25 recordings from the ApPr and 13 from the soma). Figure 1Ca shows the single-channel activity recorded at different holding potentials from the same neuron shown in **B**. From 16 cells recorded at different holding potentials, we calculated a single channel conductance of 222 ± 7.8 pS (Figure 1Cb, similar to what has been described before in CSFcNs from different species[13,14] and for the PKD2L1 channel expressed in heterologous expression systems), with an extrapolated reversal potential very close to the expected value of 0 mV (-2.2 mV). These experiments indicate that the PKD2L1-dependent single channel activity recorded from adult CSFcNs from the Gata3^{eGFP} mice is very similar to previous recordings in other transgenic mice models[14,15].

PKD2L1 channels mediate phasic and tonic currents

Dibucaine hydrochloride was described as a blocker of PKD2L1 channels in an expression system[19]. We decided to test whether dibucaine could also be used as a blocker of these channels in CSFcNs. As shown in Figure 2Aa, pressure-application of 100-200 µM dibucaine during 30 seconds strongly reduced the frequency of single channel openings, from 177 ± 163 to 5 ± 8 Hz (control vs dibucaine, respectively, Figure 2Ab, n = 12, p = 0.0005).

Apart from blocking PKD2L1 phasic activity, dibucaine had another remarkable effect. Pressure application of the drug decreased the holding current, as shown in the representative example in Figure 2Ba and **b**, where the holding current (HC) went from -23 to -10 pA. On average, dibucaine decreased the HC from -18.3 ± 9.5 to -10.5 ± 6.6 pA (Figure 2Ca, n = 13, p = 0.0002), a 44 ± 12 % reduction. Pressure application of the extracellular solution without dibucaine had no effect on either the single-channel current activity or the HC (data not shown). As expected from the effect on the HC, when the CSFcN was recorded in current-clamp, pressure application of dibucaine induced a marked hyperpolarization of the resting membrane potential (RMP, see Figure 2Bc), ffrom -66.8 ± 11.0 to -89.0 ± 14.0 mV (Fig 2Cb, n = 11, p = 0.001). Because dibucaine is a local anaesthetic it may act on other targets, like voltage-dependent sodium and calcium channels[20]. To rule-out non-specific effects of dibucaine, we performed the following experiments. First, we repeated the dibucaine application in the presence of antagonists for voltage and ligand-gated channels that may be open near the -60 mV holding potential values (TTX 0.4 µM, TEA 1 mM, 4AP 1 mM, TTAP2 20 µM, NBQX 10 µM and gabazine 10 µM to target, respectively, voltage gated Na^+, K^+ and T-type Ca^{++} channels, and the AMPA and $GABA_A$ ionotropic receptors). Under these conditions, a similar decrease in the HC was observed, from -18.1 ± 8.1 pA in control conditions to -10.8 ± 5.4 pA in the presence of the drug (Figure 2Cc, n = 11, p = 0.001), representing a 41 ± 12 % reduction. To note, there was no difference between the control HC recorded in the two conditions (without or with blockers, p = 0.9, Wilcoxon–Mann–Whitney test). Second, to rule out the possible contribution of conductances sensitive to the calcium flowing into the cell through PKD2L1 channels, we patched the neurons with the same intracellular solution + 10 mM BAPTA. Under these conditions, a decrease in the HC was still observed when pressure applying dibucaine, from -13.0 ± 5.7 pA in control conditions to -7.8 ± 2.5 pA (Figure 2Cd, n = 11, p = 0.001), a 35 ± 15 % reduction. Again, there was no difference between the control HC measured in the 3 different conditions (without blockers vs BAPTA, p = 0.17; with blockers vs BAPTA, p = 0.19, Wilcoxon–Mann–Whitney test). Such a marked effect of dibucaine on the HC and the RMP can be explained by the fact that CSFcNs are electrotonic compact neurons with a high input resistance (IR). Indeed, the IR measured from 14 somatic recordings was 1.8 ± 0.46 GΩ (Figure 2Ce; consistent with

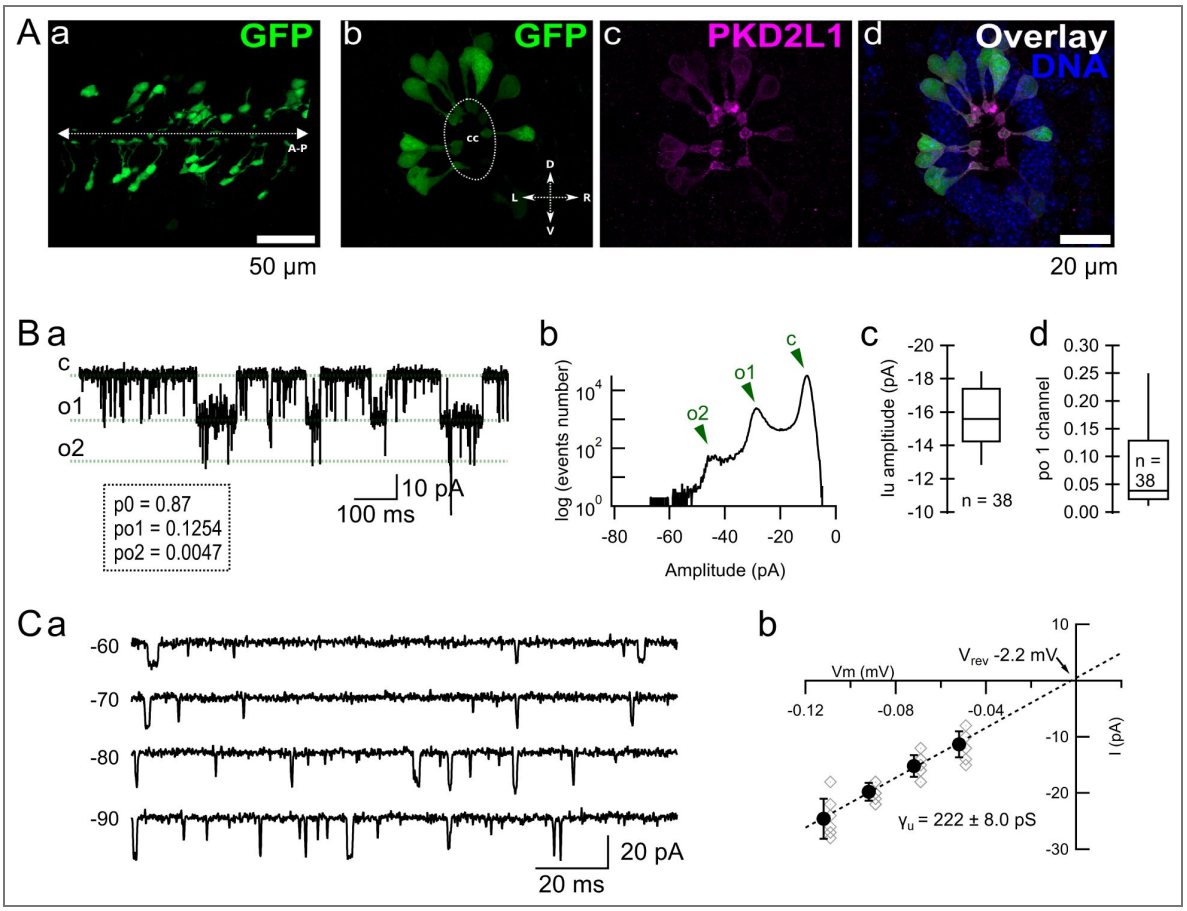

Fig 1. Characterization of PKD2L1 channel activity in CSFcNs from GATA3 mice.

Aa. Confocal image of a sagital spinal cord slice (the dissection plane passes through the CC) from a Gata3^{eGFP} animal showing the distribution of CSFcNs in the anterior-posterior (A-P) direction. **Ab, c** and **d**. Confocal image of a coronal spinal cord slice from a Gata3^{eGFP} animal showing the distribution of CSFcNs (**b**, green) around the CC (dotted line) and the immunoreactivity against the PKD2L1 channel (**c**, magenta). The overlay of the 2 channels plus the DNA (blue) are shown in **d**. In **b**, D is dorsal, V is ventral, L is left and R is right. Brightness and contrast were adjusted for display purposes. **Ba.** Spontaneous activity of a CSFcNs recorded at -60 mV at 34 °C. The inset shows the probabilities calculated for the different states of the channel. **Bb.** Histogram from the whole-cell current shown in **a**, with the 3 peaks corresponding to c, o1 and o2 indicated with arrowheads. **Bc.** Boxplot showing the unitary current amplitude measured from 38 different neurons (either somatic, n = 13, or ApPr, n = 25, whole-cell recordings). Middle horizontal line shows the median value (-15.6 pA), upper and lower horizontal lines the 75th and 25th percentiles, respectively, and top and low whisker the 90th and 10th percentiles, respectively. **Bd.** Boxplot showing the open probability measured from 38 different neurons (either somatic, n = 13, or ApPr, n = 25, whole-cell recordings). Middle horizontal line shows the median value (0.04), upper and lower horizontal lines the 75th and 25th percentiles, respectively, and top and low whisker the 90th and 10th percentiles, respectively. **Ca.** Spontaneous activity recorded at different holding potentials. **Cb.** IV relationship contructed from recordings performed at -52 (n = 9), -72 (n = 16), -92 (n = 14) and -102 mV (n = 7) holding potentials. Black symbols show averages ± SDs, and gray diamonds show individual values. The dotted line is a linear fit to the average data. From this fit an average unitary conductance of 222 ± 8.0 pS was calculated, with an extrapolated reversal potential of -2.2 mV. The Vm values have been corrected for a calculated liquid junction potential of -12 mV. In **B**, open diamonds correspond to individual neurons and filled circles to the mean ± SD.

previous published values in the turtle[21], rat[3] and mice[14,15]). As we will show later in this work, PKD2L1 channels are concentrated in the ApPr. Therefore, a better estimation of the impact of a PKD2L1-mediated current on the neuron's membrane potential should be obtained by measuring the IR directly from the ApPr. To do that we made whole-ApPr recordings, where we measured an average IR of 2.3 ± 0.5 GΩ (n = 29), statistically higher than the somatic one (p = 0.002; Figure 2Ce). Finally, we took advantage of the fact that during the slicing procedure some ApPrs are separated from the rest of the cell; these will be referred to as "isolated" ApPr (iAPr). We succeeded to record from those iApPr, where we measured an IR that was even higher than the previous values (4.4 ± 1.2 GΩ, n = 8; Figure 2Ce; $p = 6 \times 10^{-6}$, iApPr vs soma, and $p = 4 \times 10^{-7}$, iApPr vs whole-ApPr). Altogether, these results indicate that the spontaneous activity induced by PKD2L1 channels gives rise to both a phasic and a tonic current. Both phasic and tonic components of the PKD2L1-associated currents have marked effects on membrane potential as CSFcNs and, particularly, their ApPr, display very high IR values.

It has been reported that calmodulin modulates PKD2L1 channels through a direct interaction and that blocking calmodulin increases the activity of the channel[11,19,22]. In order to test whether this also applies for PKD2L1 channels in CSFcNs, we recorded channel activity under control conditions and in the presence of the calmodulin inhibitor calmidazolium. As expected, pressure-application of calmidazolium (10 or 20 μM) at the ApPr increased the channel activity, as shown in the representative recording in Supp. Figure 1Aa (top panel). The increase in channel activity is shown in the middle panel, where the slope of the plot of membrane charge as a function of time, which is dependent on the spontaneous openings of the channels, suddenly rises when calmidazolium is applied. The lower panel shows the normalized membrane charge (average ± SD) of 10 different CSFcNs before, during and after calmidazolium application. In all neurons tested (Supp. Figure 1Ab for an example), calmidazolium application also increased the HC (from -13.3 ± 5.3 to -16.0 ± 4.7 pA, n = 10, p = 0.008, Supp. Figure 1Ac), a 24 ± 20 % increase. This effect of calmidazolium on the HC had a dramatic effect on the RMP of the recorded cells. In current-clamp, calmidazolium induced a depolarization (Supp. Figure 1B), from -62.3 ± 3.3 in control conditions to -50.0 ± 5.2 mV in the presence of calmidazolium, n = 10, p = 0.002, as well as an increase in the spontaneous EPSP frequency (lower part of Supp. Figure 1Ba). This experiment shows that the increase in the activity of PKD2L1 channels impacts both phasic and tonic currents. This is consistent with our previous conclusion that blocking PKD2L1 channels likewise reduces both phasic and tonic component of PKD2L1-associated currents. Also, it highlights the importance of the intrinsic membrane properties, in this case the input resistance, in setting CSFcN excitability.

Effect of extracellular pH on PKD2L1-mediated phasic and tonic currents

We next asked whether physiological stimuli can also modulate PKD2L1 activity in a similar fashion as dibucaine and calmidazolium. To address this issue we performed changes in extracellular pH, as CSFcNs have been shown to be sensitive to changes in extracellular pH (see Introduction and further below). When a pH 6.5, 10 mM HEPES-buffered extracellular solution was pressure-applied to the ApPr, a decrease in PKD2L1 activity was observed, as shown in Figure 3Aa, **top trace**, and in the corresponding inset (traces "7.4" and "6.5"). The decrease in channel activity can be appreciated in a plot of the current charge as a function of time (Figure 3Aa, **bottom trace**). Figure 3Ab shows the normalized current integral calculated from 10 different cells before, during and after the pressure application of the acidic solution. The dotted line represents a linear fit to the first 3 seconds of the recording, which corresponds to the control period. The decrease in channel phasic activity was manifested as an increase in the closed probability of the channels (pc, Figure 2Ca, from 0.89 ± 0.09 to 0.99 ± 0.01, n = 10, p = 0.002) and a parallel decrease in the open probability of the channels (po1, Figure 2Cb, from 0.1 ± 0.08 to 0.01 ± 0.01, n = 10, p = 0.02). Meanwhile, the single channel current amplitude was not affected (-14.7 ± 1.34 vs -14.0 ± 1.7, ctrl vs pH 6.5, n = 10, p = 0.15). Apart from the effects on the phasic currents, application of the acidic solution was also accompanied by a parallel decrease in the

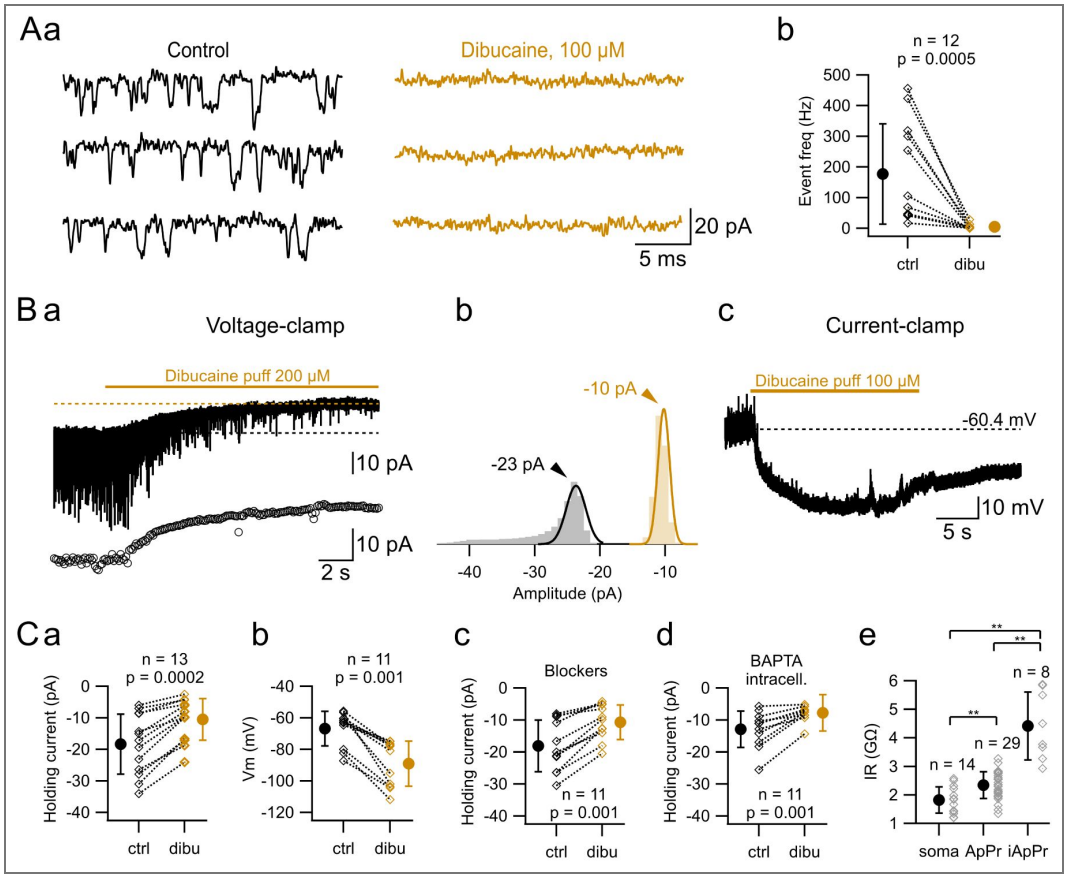

Fig 2. PKD2L1 channel activity mediates both phasic and tonic currents.

Aa. Recording of a CSFcN in control condition and during pressure application of dibucaine hydrochloride (100 µM). **Ab.** Single channel event frequency calculated in control conditions and during dibucaine application. The average frequency was reduced from 176.9 ± 163 to 5 ± 8.3 Hz (n = 13, p = 0.0007). **Ba.** Voltage-clamp recording showing how dibucaine application blocks the spontaneous events and reduces the holding current from -23 to -10 pA. The horizontal dotted lines indicate the average baseline current before and during dibucaine application. The bottom trace shows the average current value calculated from 100 ms time-periods, where the reduction in the holding current can be readily appreciated. **Bb.** Histograms of the recorded current during the control (black) and the dibucaine (orange) time periods. The data has been adjusted with a gaussian function (continuous lines). The mean values of the Gaussian fits correspond to the holding current values shown in **Ba** (dotted lines; -23 and -10 pA, control and dibucaine, respectively). **Bc.** Current-clamp recording showing the hyperpolarisation induced by dibucaine application, from -60.4 to -95 mV in this example. **a** and **c** correspond to different neurons. **Ca.** Effect of dibucaine pressure application on the HC: -18.3 ± 9.5 in control to -10.5 ± 6.6 pA in dibucaine (n = 13, p = 0.002). **Cb.** Effect of dibucaine application on the resting membrane potential: -66.8 ± 11.0 in control to -89.0 ± 14.0 mV in dibucaine (n = 11, p = 0.001). **Cc**. Effect of dibucaine pressure application on the HC in the presence of voltage-gated and ionotropic channels blockers: -18.1 ± 8.1 pA in control to -10.8 ± 5.4 pA in dibucaine (n = 11, p = 0.001). **Cd.** Effect of dibucaine pressure application on the HC in the presence of 10 mM BAPTA in the internal solution of the recorded neurons: -13.0 ± 5.7 pA in control to -7.8 ± 2.5 pA in dibucaine (n = 11, p = 0.015). **Ce.** IR values calculated from somatic (1.8 ± 0.46 GΩ, n = 14), ApPr (2.3 ± 0.48 GΩ, n = 29) and isolated ApPr (4.4 ± 0.12 GΩ, n = 8) recordings. p = 0.002, soma vs whole-ApPr; $p = 6 \times 10^{-6}$, iApPr vs soma and $p = 4 \times 10^{-7}$, iApPr vs whole-ApPr. In **Ab** and **C**, diamonds correspond to individual neurons and circles to the mean ± SD. Statistical comparison between groups was performed with a Wilcoxon signed-rank test for paired data (**Ab** and **Ca** to **d**) and a Wilcoxon–Mann–Whitney for unpaired data (**Ce**).

recorded HC, from -16.8 ± 6.7 to -12.0 ± 5.2 pA (Figure 3Cc, n = 10, p = 0.002), a 28.6 ± 12.7% reduction. The effect on the holding current can be seen in the VC recordings shown in Figure 3Aa, top, but is more clearly seen when the recorded current is averaged over 100 ms time periods (Figure 3Aa, middle graph). When the cell was held in CC, pressure application of the pH 6.5 solution produced a marked hyperpolarization of the RMP (Figure 3B for an example), from -64.5 ± 5.2 to -76.0 ± 3.4 mV (n = 8, p = 0.008; Figure 3Bd). In 3 out the 8 experiments, a quickly desensitizing inward current was observed in VC at the onset of the application of the acidic solution (Supplementary Figure 2Aa), which produced a short-lasting depolarization in CC that was followed by the persistent hyperpolarization described above (Supplementary Figure 2Ab). As previously described[14], this current probably reflects the opening of ASIC channels. This current was not further characterized.

On the other hand, when a pH 8.4 HEPES-buffered extracellular solution was pressure-applied, a clear increase in PKD2L1 activity was recorded (Supplementary Figure 3A and B). This was manifested as an increase in the current integral (Supplementary Figure 3), a decrease in the closed probability of the channels (from 0.96 ± 0.036 to 0.76 ± 0.13, n = 8, p = 0.008, Supplementary Figure 3Da) and an increase in the open probability of the channels (from 0.042 ± 0.034 to 0.2 ± 0.01, n = 8, p = 0.008, Supplementary Figure 3Db). As expected, there was also a slight increase in the HC (from -11.7 ± 7.3 to -15.2 ± 7.9 pA, n = 8, p = 0.008, Supplementary Figure 3Dc) and a depolarization of the RMP (from -75.2 ± 7.0 to -66.2 ± 10 mV, n = 6, p = 0.03, Supplementary Figure 3Dd). The single channel current remained unchanged (-16.85 ± 0.95 vs -17.3 ± 1.0 pA, ctrl vs pH 8.4; respectively, n = 8, p = 0.45).

The experiments presented so far indicate that the basal activity of PKD2L1 channels plays a central role in regulating CSFcNs excitability. This regulation takes place at two levels: by a modulation of the phasic activity of the channels, as has already been described[14,15], and also by a modulation of a novel PKD2L1-dependent tonic current that has a dramatic effect in setting the RMP in CSFcN. In this sense, PKD2L1 basal activity determines an excitability set-point that can be up and down-regulated by small pH changes. This is clearly seen when plotting po as a function of pH (Figure 3Ce). The experimental data has been fitted by a Hill equation that shows a pH half-value of 8.1 ± 0.04, very close to physiological pH and to previously estimated values in expression systems[23] and computational model[24]. A similar result is obtained when plotting the holding current change (in relation to the control value at pH 7.4) as a function of pH. Fitting the data with a Hill equation gives a pH half-value of 7.5 ± 0.02 (Figure 2Cf). In order to better appreciate the effect of the HC on the Vm, we calculated the Vm and the HC differences produced (in individual neurons) by the different experimental challenges tested here, and then plotted the Vm vs the HC difference. The plot, shown in Figure 3D, indicates a strong correlation between the 2 values. The fit of the data with a linear function (dotted gray line) indicates a slope value of 2.3 GΩ, very close to the IR values calculated for the ApPr (Figure 1Ee). Taken together, these data indicate that both the PKD2L1 channel po and the holding current are very sensitive to extracellular pH changes, that the maximal pH sensitivity occurs within the physiological range and that small changes in the tonic current can have a substantial effect on CSFcNs RMP (≈ 2.3 mV/pA).

The use of laser photolysis to assess the pH sensitivity of CSFcNs

It has been reported that the sensitivity of CSFcNs to pH changes depends on the activity of two different channels, PKD2L1 and ASICs. Those studies used a combination of electrophysiological methods with bath or pressure applications of drugs, but these strategies suffer from limited spatial resolution, preventing precise localization of channel activity within the CSFcN membrane. To overcome this limitation and to precisely map the sub-cellular sensitivity to pH of the different CSFcN compartments, we employed laser photolysis, as this approach provides high spatial resolution (the laser can be focused to a small spot, with x-y dimensions of 1.5 μm[25,26]) as well as a high temporal resolution (the laser can be switched on and off very rapidly, thus producing almost instantaneous agonist changes). This is shown schematically in Figure 4A-B. Briefly, after the

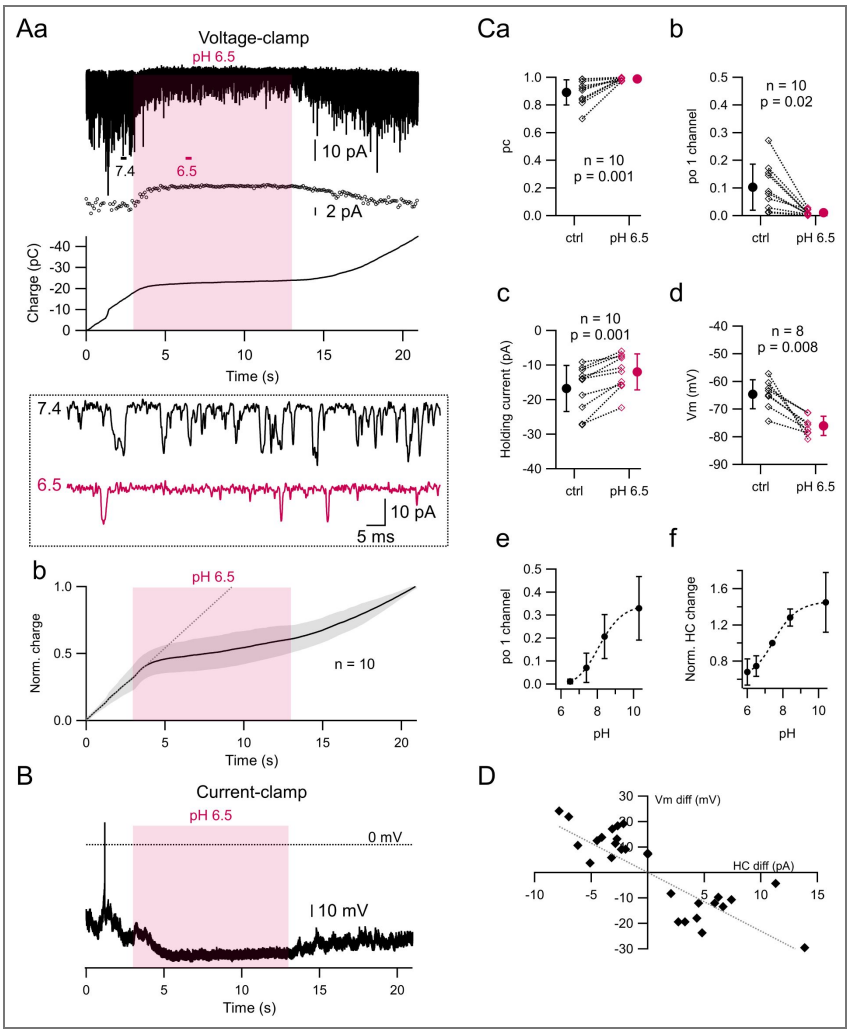

Fig 3. pH sensitivity of PKD2L1-mediated phasic and tonic currents.

Aa. Top. Spontaneous PKD2L1 channel activity recorded in a CSFcN at a -60 mV holding potential. A pH 6.5 solution was pressure-applied during 10 s (starting at 3 s, red area). **Middle.** Holding current calculated from the recording shown on the top. **Bottom.** Membrane charge calculated from the recording shown on the top. **Inset.** Segments **7.4** and **6.5** in **Aa** are shown with expanded time and amplitude scales in order to see the decrease in the spontaneous single channel activity during the application of the acidic solution, without any change in the single channel current. **Ab.** Mean membrane charge ± SD calculated (gray surface) from 10 neurons tested in the same conditions as the cell shown in **a**. The dotted line corresponds to a linear fit to the control period (first 3 seconds of the recording). The application of the acidic solution produces a clear decrease in the slope of the membrane charge, indicating a decrease in the spontaneous openings of the channels. **B.** Same experiment as in **a**, but the spontaneous activity was recorded in current-clamp. The application of the acidic solution produces a hyperpolarization of the RMP (from -57.2 to -80 mV in this example). **Ca.** Effect of the pH 6.5 solution application on the close probability, pc: 0.89 ± 0.09 in control conditions vs. 0.99 ± 0.01 in the pH 6.5 solution (n = 10, p = 0.001). **Cb.** Effect of a pH 6.5 solution application on po1: 0.1 ± 0.08 in control conditions vs. 0.01 ± 0.01 mV in the pH 6.5 solution (n = 10, p = 0.02). **Cc.** Effect of a pH 6.5 solution application on the holding current: -16.8 ± 6.7 in control conditions vs. -12.0 ± 5.2 pA in the pH 6.5 solution (n = 10, p = 0.001). **Cd.** Effect of a pH 6.5 solution application on the resting membrane potential: -64.5 ± 5.2 in control conditions vs. -76.0 ± 3.4 mV in the pH 6.5 solution (n = 8, p = 0.008). **Ce.** po1 as a function of pH. N = 10 for pH 6.5, 25 for pH 7.4, 8 for pH 8.4 and 7 for pH 10.4. The dotted line shows the fitting of the data to a Hill equation that yields a half pH value of 8.1 ± 0.04. Error bars are SDs. **Cf.** Holding current change (HC test/HC at pH 7.4) as a function of pH. N = 5 for pH 6, 5 for 6.5, 6 for pH 8.4 and 7 for pH 10.4. The dotted line shows the fitting of the data to a Hill equation that yelds a half pH value of 7.5 ± 0.02. Error bars are SDs. In **C**, diamonds correspond to individual neurons and circles to the mean ± SD. **D.** Relationship between Vm and HC differences recorded in 28 individual neurons. The 2 variables are strongly correlated (Spearman rank correlation coefficient = -0.77). The dotted gray line is a fit with a linear function (ax + b, where b = 0), which shows a slope of 2.3 ± 0.3 GΩ. In **C**, statistical comparison between groups was performed with a Wilcoxon signed-rank test.

different CSFcN compartments (soma, dendrite and ApPr) were identified by fluorescence of Alexa 594, the focus of the objective was positioned in the targeted compartment (ApPr in the example in Figure 4A), where laser photolysis was evoked.

To induce pH changes we used the glutamate cage MNI-glutamate, as its photolysis generates the stoichiometric release of one glutamate molecule together with one proton[27] (Figure 4B, top reaction). MNI-glutamate uncaging in the ApPr of CSFcNs elicited two currents with different characteristics. A first component had very quick rise and decay times (values of the example shown in Figure 4C: amplitude 38 pA, 10-90 % risetime 0.86 ms and decay time constant 2.6 ms; see inset for details). It appeared immediately after the laser pulse (magenta arrowhead in Figure 4C) and fluctuated little among repetitions. A second component was indistinguishable from the PKD2L1-dependent spontaneous activity recorded above. It followed the laser pulse with variable latencies (although always longer than the latencies of the first component) and fluctuated widely among repetitions. The first current was blocked by $AMPA_R$ antagonists (NBQX or CNQX) and was therefore attributed to AMPA receptor activation. The second component of the response was spared by both AMPA or $NMDA_R$ blockers (the experiments shown in Figures 4D and **G** were done in the presence of NBQX and APV) and was presumed to reflect the pH change. To confirm that this current resulted from the release of protons (and not glutamate), we used the caged compound MNI-γLGG which has the same photochemistry as MNI-glutamate except that it releases the inactive enantiomer of the $AMPA_R$ antagonist γDGG[28] together with a proton (Figure 4B, bottom reaction). This failed to produce the short latency current, but produced the same long latency current as above, indicating that the late current is related to proton release rather than glutamate (Figure 4B for an example). Also, no current could be observed when the ApPr was illuminated in the absence of a caged compound (data not shown), indicating that the current is not due to a light artifact or to photodamage.

The proton-induced current is an off-current

Inspection of the experimental traces presented in Figure 4C suggests that the photolysis of an MNI-cage in the ApPr of CSFcNs increases the probability of channel opening with a characteristic long latency. The increase in channel activity was analysed in two ways. First, the membrane charge was calculated from spontaneous recordings (gray traces in Figure 4D) and from recordings where MNI-glutamate (or MNI-γLGG) was photolysed (black traces in Figure 4D). As already mentioned (Figure 3), the membrane charge calculated from spontaneous sweeps shows a linear increase as a function of time, whereas that calculated from laser-evoked sweeps shows a sudden slope increase induced by the laser pulse, that recovers later. Figure 4E shows the average normalized membrane charge (black trace) calculated from 14 different neurons where photolysis was evoked on the ApPr. The data was fitted with the sum of a linear and exponential functions. The time constant of the exponential function, τ, is equal to 258 ms. The magenta-shaded area in the graph (in Figure 4E) spans 500 ms ($\approx 2\ \tau_s$), representing the estimated lifetime of the photolysis-induced increase in channel activity. Second, we measured channel probabilities from spontaneous recordings and compared them to those during the magenta-shaded time-window, which corresponds to the photolysis effect (see above). This analysis indicated that the opening probability increased (Figure 4Fa) and the closing probability decreased (Figure 4Fb) as a result of the photolysis.

As previously mentioned, the increase in channel activity does not happen during the laser pulse but a few milliseconds afterwards. In this sense, the latency difference between the AMPA-dependent and proton dependent components is striking. This difference can be clearly appreciated in the inset in Figure 4C, where the AMPA-dependent component coincides with the laser pulse (magenta trace) whereas the proton-dependent component appears more than 30 ms later. The PKD2L1 current latency in sweep #4, which is the shortest among the 5 repetitions, is 11 ms. To characterize the latency distribution of the PKD2L1-mediated single currents relative to laser pulse timing, we measured the current onset times from idealized traces during 2-second recording periods (see Figure 4Ga for an example; experiments done in continuous presence of NBQX or with MNI-γLGG). To minimize contamination from spontaneous channel openings, we

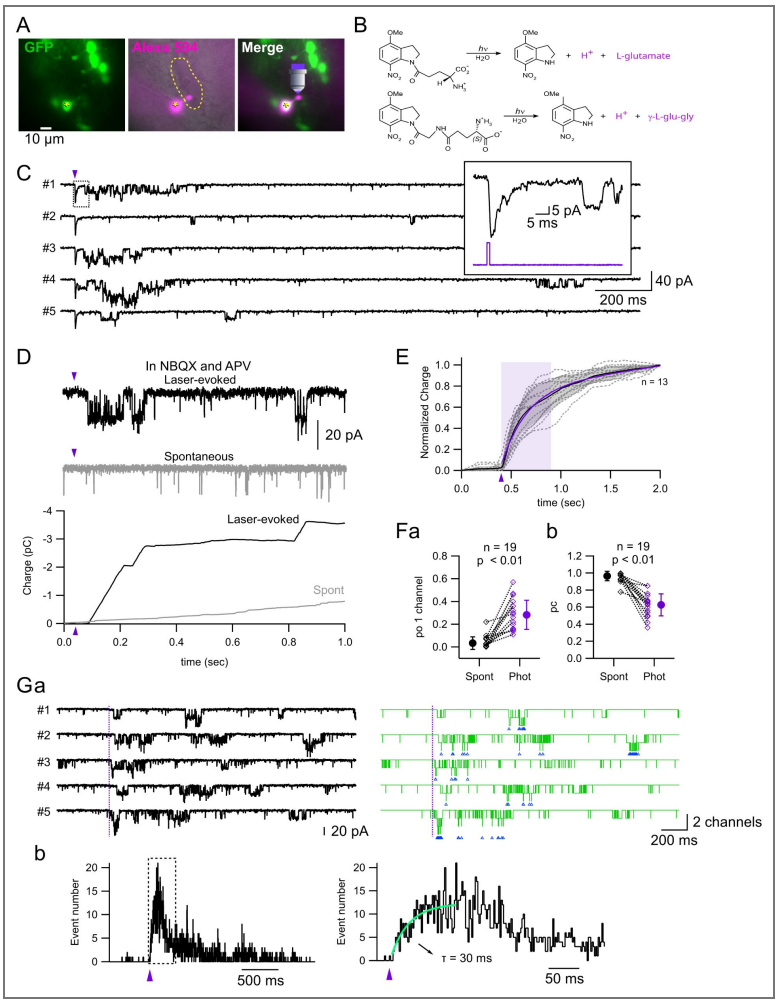

Fig 4. Proton photolysis induces an off-current in CSFcNs.

A. Schematic of the experiment. Pictures showing the eGFP fluorescence (left), the Alexa 594 fluorescence (middle) and the merging of the 2 channels (right). The yellow star indicates the recorded cell, and the objective the location of the targeted compartment. The yellow dotted line shows the approximate boundaries of the central canal. **B.** Schematic of the photolysis reaction shown for the 2 caged compounds used: MNI-Glutamate (top) and MNI-γLGG (bottom). **C.** 2 second-long recordings showing the typical response of a CSFcN (shown in **A**) to the photolysis of MNI-Glutamate on the ApPr. The photolysis (magenta arrowhead; 2 mW, 500 µs duration) was repeated 5 times with 10 seconds intervals. The inset shows sweep #1 in an expanded scale in order to appreciate the fast kinetics of the $AMPA_R$-mediated current. The magenta, bottom trace, represents the timing of the laser pulse (which is measured with a photodiode in the laser path). **D. Top.** The black trace shows the current evoked by a 500 µs laser pulse and the gray trace the spontaneous current recording in the same CSFcN. **Bottom.** Membrane charge calculated from the above recordings. **E.** Normalized (to the 2 s value) membrane charge as a function of time. Black trace shows the average, gray area the SD and dotted traces individual experiments (n = 13). The magenta continuous line represents the fit of the average curve with the sum of a linear + an exponential function representing the increase evoked by the photolysis and the linear increase due to the spontaneous channel openings, respectively (see methods). The τ of the exponential function was 258 ± 2 ms. The x-span of the magenta area represents 500 ms (≈ 2 τs). **Fa.** po1 calculated from spontaneous recordings (0.03 ± 0.06) and during the time depicted in the magenta area shown in **E** (0.28 ± 0.13) from 19 different cells. **Fb.** pc calculated from spontaneous recordings (0.97 ± 0.06) and during the magenta area shown in **E** (0.63 ± 0.13) from 19 different cells. In both cases, the differences were statistically significant. **Ga.** Example of laser-evoked currents (left, black traces) and the corresponding idealized events (right, green traces). MNI-γLGG was used in this experiment. The blue arrowheads below each idealized trace indicates the timing of double events (where 2 channels opened simultaneously). Vertical, magenta dotted lines indicate the laser pulse (500 µs). **Gb.** Latency distribution of double events (95 photolysis repetitions from 20 neurons) shown with 2 different time resolutions (the graph on the right corresponds to the time indicated by the dotted rectangle on the graph on the left). The rising phase of the histogram has been fitted with an exponential function (green trace) that has a τ of 30 ± 12 ms. The magenta arrowheads indicate the timing of the laser pulse. In **F**, statistical comparison between groups was performed with a Wilcoxon signed-rank test.

only considered double events (simultaneous opening of two channels) as the spontaneous occurrence of such events is very low. From the onset times of these double events, we constructed the latency distribution histogram shown in Figure 4Gb. The open probability gradually rises after the laser pulse, with a time constant of 30 ± 12 ms, peaking at 108 ms after the laser pulse. This analysis, together with our calculation that photolysis induces a transient pH drop of around 4 units (from 7.4 to ≈ 3.3) that returns to baseline in microseconds (see materials section), indicates that the photolysis-evoked PKD2L1 single-channel currents represent, in fact, an off-response. Indeed, it has been shown that PKD2L1 channels, which are activated by alkali and inhibited by acid, are also activated by acid removal[24,29,30], giving rise to the so-called off-response.

The off-current is mediated by the activation of PKD2L1 channels

The experiments presented in the previous section suggest that the off-current is mediated by PKD2L1 channels. To confirm this possibility, we performed the following experiments/analysis. Firstly, channel activity was blocked when the photolysis is performed in the continuous presence of dibucaine. This can be appreciated in the representative trace shown in Supplementary Figure 4A: in the presence of dibucaine (gray trace), both the spontaneous currents and the laser-evoked currents were blocked. The bottom panel shows the time-dependent current integrals calculated from the upper traces. Supplementary Figure 4B shows the average normalized membrane charge recorded under two conditions, control (n = 14 neurons, same graph as in Figure 4E) and dibucaine (n = 6 neurons). Some of the experiments in the presence of dibucaine were done in the absence of $AMPA_R$ blockers. In these cases, a clear fast, inward, $AMPA_R$-mediated current can be appreciated which is not followed by any single channel event (Supplementary Figure 4D), indicating that the lack of response was not due to an unresponsive or damaged ApPr.

Secondly, the single channel current evoked by the laser pulse (calculated during the 2 τ_s time window after the laser pulse; see above) was indistinguishable from that obtained during the spontaneous current activity (Supplementary Figure 4C, -16.7 ± 2.0 to 17.0 ± 2.0 pA, n = 21, p = 0.54).

ASICs have been shown to be present in CSFcNs[13–15,31]. To rule out any contribution of ASIC to the photolysis-induced response, we performed the experiment in the continuous presence of the ASIC blockers PsTx (100 nM) and ApeTx2 (100 nM). In these conditions, neither the single channel events nor the charge increase evoked by photolysis were affected (Supplementary Figure 4E), confirming that the increase in channel activity related to the release of protons by photolysis on the ApPr is dependent on the activation of PKD2L1 channels.

The PKD2L1-mediated current is generated in the ApPr

The next series of experiments was designed to assess the spatial sensitivity of CSFcNs to pH changes. To this aim, we photolysed MNI-compounds in different CSFcNs compartments. Figure 5A shows the result of an experiment where the photolysis of MNI-γLGG was performed either in the ApPr, the soma or 5 μm away from the ApPr (Figure 5Aa). As expected, photolysis in the ApPr induced the typical off-current, characterized by the increase in the unitary activity of PKD2L1 channels (Figure 5Ab, black traces) as well as in membrane charge; on the contrary, photolysis in the soma (Figure 5Ab, pink traces) or in the dendrite (data not shown) did not produce a sizable increase in the unitary currents. Figure 5Ac summarizes the photolysis-induced changes on the membrane charge. Photolysis on the ApPr elicited a pronounced increase in membrane charge, whereas photolysis in the soma produced no detectable change. Notably, the response to photolysis in the soma was indistinguishable from the photolysis 5 μm away from the ApPr (magenta vs green traces, respectively), which is more evident in the bottom panel showing the same data set in an expanded amplitude scale.

To further assess the sensitivity of ApPrs to pH changes, we exploited the fact that during the slicing procedure some ApPrs are separated from the rest of the cell. We term these cell fragments iApPrs. The iApPr were filled with Alexa 594 in order to confirm that they were indeed detached from the rest of the neuron (Figure 5Ba). Interestingly, iApPrs show single-channel currents

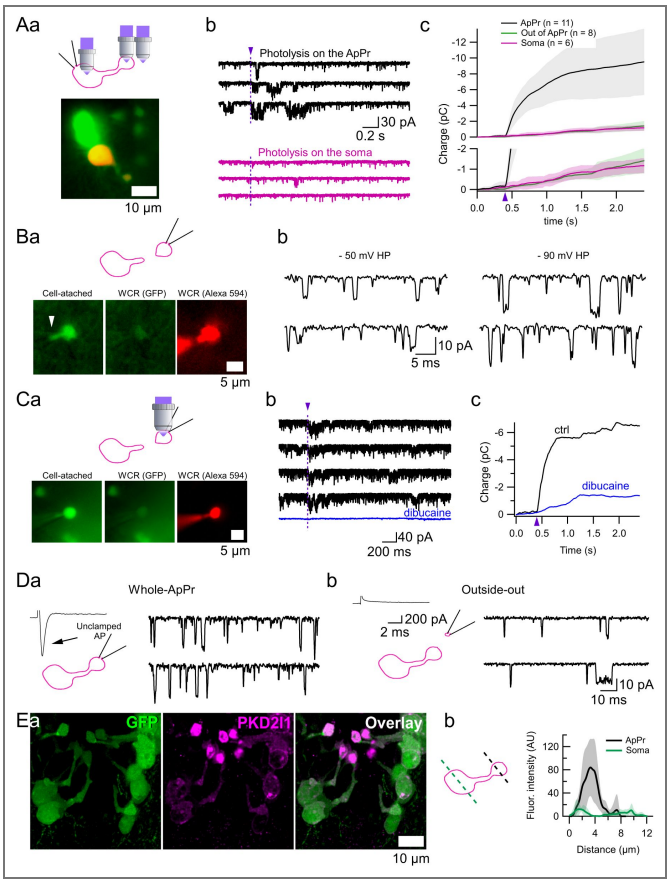

Fig 5. PKD2L1 channels are segregated to the ApPr.

Aa. Top. Schematic drawing showing the different photolysis locations. **Bottom.** Superimposition of pictures showing the eGFP (green) and the Alexa 594 (red, which corresponds to the recorded cell fluorescence. **Ab.** Representative sweeps showing the membrane currents recorded when the photolysis of MNI-γLGG was performed either on the ApPr (black traces) or on the soma (magenta traces). **Ac.** Average membrane charge calculated from recordings corresponding to the photolysis of MNI-γLGG or MNI-glutamate in different locations. Shaded areas correspond to ± SDs. Bottom graph shows the same traces but in a different amplitude scale. **Ba. Top.** Schematic drawing of experimental design. Whole-cell recordings were performed from iApPrs. **Bottom.** Pictures showing the different recording configurations: **left** in cell-attached, where the eGFP green signal can be seen inside the recording pipette as the ApPr membrane goes into the pipette when the positive pressure used for patching is released; **midddle** in whole-cell a few seconds after break-in, where it can be seen that the green eGFP fluorescence has already washed-out; **right** in whole-cell, where the morphology of the isolated ApPr can be appreciated by the red Alexa 594 fluorescence. **Bb.** Whole-cell recordings from the isolated ApPr shown in **a** at two different holding potentials, -50 and -90 mV. A clear PKD2L1-dependent spontaneous activity can be seen. HP: holding potential. **Ca. Top.** Schematic drawing of experimental design. The photolysis was produced on an isolated ApPr. **Bottom.** Pictures showing the different recording configurations. Same as **Ba**. **Cb.** Whole-cell recordings from the isolated ApPr shown in **a** and its response to photolysis. The black traces are in control conditions and the bottom, blue trace in the presence of 100 µM dibucaine. **Cc.** Average membrane charge calculated from the recordings shown in **b**. **D.** Recordings from an ApPr in the whole-cell configuration (**a**) and in the outside-out configuration (**b**). The traces on the left show the current responses to a 50 ms depolarization to -10 mV from a -60 mV holding potential. This voltage pulse induces an unclamped sodium spike in whole-cell but no response in outside-out, confirming that the outside-out patch has completely detached from the ApPr (as isolated ApPr do not have sodium currents). PKD2L1 activity is still present in the outside-out recording. **Ea.** Maximum intensity projection of 41 deconvolved optical sections spaced by 130 nm. CSFcNs expressing eGFP (green, left panel), which also express PKD2L1 receptors (magenta, middle panel.). The overlay of the 2 channels is shown on the right panel. The dotted white line in the left, GFP panel, indicates the distance along which the density plots shown in **b** were constructed. **Eb.** Density plots depicting anti-PKD2L1 mean fluorescence intensity (trace) ± SDs (shade) measured at the soma (green) and in the ApPr (black). n = 6 for each compartment. The fluorescence mas measured along the dotted green and black lines shown in the scheme. The maximal mean intensity is 84 for the ApPr and 12.5 for the soma. Brightness and contrast were adjusted for display purposes. Unsaturated images were used for quantification. In **A** and **C**, the vertical dotted lines and magenta arrowheads correspond to the timing of the photolysis pulse.

with the same single-channel conductance and voltage-dependence as non-isolated ApPrs, as can be appreciated in the representative example shown in Figure 5Bb. Furthermore, iApPrs respond to proton photolysis similarly to non-isolated ApPrs (Figure 5C) and both the spontaneous single-channel activity as well as the photolysis-induced charge increase are blocked by dibucaine (Figure 5Cb-c).

To confirm the presence of PKD2L1 channels in ApPrs, we performed outside-out recordings from patches of membrane taken from the ApPr (Figure 5D). We first recorded the ApPr in the whole-ApPr configuration and then slowly took out the pipette until no unclamped action current could be seen (as iApPrs do not show voltage-gated sodium currents; Figure 5Da-b). PKD2L1 channel openings were observed in the outside-out configuration (Figure 5Db), albeit with a lower opening frequency than in the whole-cell configuration (Figure 5Da). Such single-channel activity was observed in 6/10 outside-out recordings.

Finally, we performed immunohistochemical experiments to characterise the location of the PKD2L1 protein in Gata3^{eGFP}. As seen in Figure 5E, the PKD2L1-related fluorescence intensity (shown in magenta in Figure 5Ea) is >6-fold higher in the ApPr than in the soma (Figure 5Eb) or dendrite (not shown). The mean fluorescence in the ApPr was 84 ± 49 AU and dropped to 12.5 ± 8 AU in the soma. Altogether, our experiments indicate that the PKD2L1 channels are specifically enriched in the ApPr. Although we cannot rule out the presence of PKD2L1 channels in other compartments, our electrophysiological and immunohistochemical experiments suggest that functional PKD2L1 channels are topologically segregated to the ApPr.

Discussion

The pH sensitivity of neurons depends on both their anatomical features and the functional properties of their ion channels. As all neurons exhibit some degree of pH sensitivity[32], investigating it needs the use of targeted techniques that can accurately assess both the anatomical and physiological properties of the channels involved in the response to pH. Our data, derived from the integration of whole-ApPr and outside-out recordings, along with laser photolysis of protons and immunohistochemistry, demonstrates that the unique ability of CSFcNs to function as precise CSF pH sensors arises from the distinct physiological properties of PKD2L1 channels and, crucially, their spatial segregation within the ApPr. These finding highlight how specialized anatomical and physiological features enable selective pH sensing.

From the anatomical standpoint, the functional evidence gathered here by combining whole-ApPr and outside-out recordings with laser-photolysis of protons and immunohistochemistry indicates that PKD2L1 channels are predominantly located in the ApPr. This is an important finding that highlights the role of the ApPr as a sensory compartment. In this work we show that when recording from CSFcNs a PKD2L1-mediated off current is evoked when uncaging protons on the ApPr, but not when uncaging on the dendrite or the soma. As expected, uncaging a few microns away from the ApPr is inefficient to trigger a response, which confirms the high spatial resolution of the technique[25]. The other experiments presented in Figure 5 point to the same direction: i. outside-out recordings from the ApPr show PKD2L1-dependent single channel activity; ii. whole-cell recording from isolated ApPrs show single-channel currents that are indistinguishable from those recorded from intact ApPrs; iii. photolysis on isolated ApPr evokes off-currents as in intact cells; iv. immunohistochemical experiments show that PKD2L1 expression is higher in the ApPr than in the soma (see also[33]). Although we have not attempted to do outside-out patches from somatic recordings, single channel recordings in this configuration has proved to be difficult by another group[14]. It is interesting to analyse this anatomical segregation of the receptors in the context of previous electron microscopy data, which shows that in the intact spinal cord a tight cytoskeleton ring (mainly adherens and tight junctions) formed by the ependymal cells[34,35] isolates the ApPr from the rest of the spinal parenchyma. Interestingly, it has been shown that the ionic composition of the CSF is different from that in the serum[36]. This implies that the ApPr and the soma are exposed to different extracellular solutions, with a potential impact on the equilibrium potentials of the main ions involved in the CSFcNs electrical response. Although in our

slice preparation the interphase separating the CSF from the spinal cord parenchyma is lost, it makes sense that the ApPrs are immersed in the CSF and physically separated, as they should if they are to sense CSF composition.

The physiological features of PKD2L1 channels need also to be taken into account to fully understand the role of CSFcNs as pH sensors: i. PKD2L1 channels are extremely sensitive to proton concentration in the physiological range. This has been quantified by González-Perrett et al.[23], who showed that the equilibrium constant for the related PKD2 channel expressed in lipid bilayers is 6.4 (see also[24]). At this pH value the open probability of the channel is half of its maximum. We performed the same analysis (Figure 3Ce) and obtained a value close to 8.0. Interestingly, the holding current can also be used as a proxy of the channel sensitivity to pH changes (Figure 3Cf). The fact that physiological pH indicates the half-maximum of the conductance state of PKD2L1 channels activation curve defines their second physiological feature; ii. PKD2L1 channels are able to sense deviations of the pH in both directions, either by decreasing (acidification) or increasing (alcalinisation) the channel open probability. Enhanced excitability of CSFcNs resulting from increased PKD2L1 activity has been shown in mice[15] and lamprey[13], and has been attributed to augmented phasic activity of the channel. Remarkably, the fact that a decrease in channel activity can also provide meaningful information to the cell by inducing a strong hyperpolarization has not been described before. This exquisite sensitivity of the cell's RMP to small changes in the membrane current can be explained by the high input resistance of the ApPr, which we have quantified here by performing direct recordings from that compartment; iii. finally, the physiological effects of PKD2L1 channels are achieved in part through the modulation of a tonic current. This makes the channel particularly well-fitted to act as a sensor of more or less slow pH variations. Indeed, the pH of the CSF does not change phasically within the millisecond time-range, as does the pH[37] or the neurotransmitter concentration[38] in the synaptic cleft, but rather in a slower fashion that requires special channels to transduce these slow and probably long-lasting changes.

The tonic current

In GABAergic systems, two different types of $GABA_A$ receptors mediate phasic and tonic currents: one depends on the activation of low-affinity receptors by synaptically released GABA, while the other depends on the activation of high-affinity $GABA_A$ receptors by low concentrations of ambient GABA[39]. In this work we describe phasic, single-channel currents that depend on the spontaneous opening of PKD2L1 channels, and a type of tonic current that was made evident when PKD2L1 channels were blocked with dibucaine. The following experimental evidence indicates that both the phasic, single channel events, and the tonic current depend on the same channel: first, the effect of dibucaine persists when blocking voltage-dependent and ligand-gated channels that may also contribute to the appearance of a tonic current; second, the effect of dibucaine was still present when recording CSFcNs with an IS containing a high concentration of BAPTA; third, the tonic current was modulated by other exogenous (calmidazolium) and endogenous (pH) modulators that are known to affect PKD2L1 channels. These experiments suggest that, apart from the closed and open states of the channel, some other conducting state of the channel may exist as well. Alternatively, very short opening periods of the channels, not seen in the recordings but nevertheless present and blocked by dibucaine, could also explain the tonic current. The assesment between these two putative mechanisms is beyond the scope of this work.

The magnitude of the tonic current compared to the spontaneous, phasic currents, is substantial. The average single channel current measured in this work is ≈ -16 pA and po is ≈ 0.04, which determines a mean phasic current of 16 pA × 0.04 = 0.64 pA. On the other hand, the average tonic current (Figure 2Ca) is ≈ 8 pA. Altogether, the percentage of tonic and phasic currents are roughly 90 % and 10 %, respectively, which highlights the importance of the tonic current in the physiology of CSFcNs.

The off-response

It has been reported previously that PKD2L1 channels are responsible for an off-response when challenged by acidic solutions[24,29,30,40]. A first indication of the presence of an off-current in CSFcNs was provided by Orts-del'Immagine[14], who reported in some of the recorded neurons an increase in the frequency of single channel events after pressure applying a pH 2.8 solution. In this work we provide a detailed analysis of the off-current by using laser photolysis of protons and further show that the current is only evoked when uncaging at the ApPr, indicating that functional PKD2L1 channels are located there (see above). In the published literature the off-response appears with large-scale acidifications, in the order of several pH units. In this paper we have likewise induced substantial pH changes (to 3 or 3.5; see **Methods**) but have not attempted to quantify the pH dependence of the off-current. It is nevertheless interesting to highlight the fact that the off-current does not require long-lasting changes in the extracellular pH to develop. Instead, very brief pH changes are enough, which opens the possibility that the ApPrs may also respond to sudden ACSF acidifications, as may occur during neurosecretion[41]. It would be interesting in the future to explore with photolysis the concentration and time dependence of the off-current (for example, smaller pH changes but longer pulses) in order to assess its physiological significance.

ApPrs do not have sodium currents

The possibility of recording from iApPrs allowed us to make a serendipitous finding: ApPrs do not have active sodium conductances. This is not surprising as many CNS neurons do not have active conductances in their dendrites but is nevertheless interesting as the voltage deviations that occur in the ApPr need to propagate down the soma (and probably the axon) in order to have impact on the spike triggering zone. The fact that the ApPr and the soma are electrotonically close, as shown by Orts-Del'immagine and collaborators[15], certainly facilitates this propagation. It would be interesting in the future to investigate specifically what are the voltage-dependent conductances to be found in the ApPr. In any case, the high IR of isolated ApPrs is probably an indication of the low density of active conductances in this neuronal compartment.

The involvement of ASIC

ASICs, also known as proton-gated channels, play important physiological and pathological roles in the nervous system[37,42]. In CSFcNs, ASICs have been reported as mediating part of the response to acidification[13–15,31]. In this study, we observed in a few cells a rapidly desensitizing inward current when pressure applying a pH 6.5 solution, and occasionally an inward current with similar characteristics when uncaging either MNI-Glu or MNI-γLGG at the soma (Supplementary Figure 2B). However, we never saw such an inward current when photolysing at the ApPr, and the off-response evoked by the photolysis of protons on the ApPr was not affected in the presence of ASIC channel blockers (supplementary Figure 3). As ASICs are widely expressed in many brain areas and neuronal compartments[32], the most parsimonious explanation for these experimental results is that the ASIC-dependent current recorded in CSFcNs results from the activation of somatic ASICs, but that those channels are not present in the ApPr. ASICs may be suited to sense changes in the pH of the parenchyma by CSFcNs. The pH sensitivity of CSFcNs is thus a complex response that depends on different channels localized in different neuronal compartments. Our results indicate that the sensitivity of CSFcNs to changes in the pH of the ACSF is solely dependent on the modulation of PKD2L1 channels.

Materials and methods

Transgenic mice

Gata3^{eGFP} mice were generated using bacterial artificial chromosome (BAC) recombination as described[43]. The eGFP gene was inserted by deleting 286 bp of coding sequences from the first exon. The sequences flanking the insertions were: 5'agccgaggac-eGFP–cgtggaccca3'. Four Gata3-

eGFP founder lines were generated that expressed eGFP in an identical manner to GATA3 in the spinal cord. One of these lines was selected for this study. Animals of either sex were maintained in a 12 hs. light/dark cycle with food and water *ad libitum*, humidity between 50 and 60%.

Slice preparation for electrophysiological experiments

Spinal cord slices were obtained from $Gata3^{eGFP}$ mice aged 30 to 45 days old. Slices were prepared as previously described[3]. Briefly, mice were decapitated under isoflurane anesthesia following approved ethical procedures (CEUA 001/01/2022a) and the spinal cord dissected in an ice-cold artificial ACSF of the following composition (in mM): 101 NaCl, 3.8 KCl, 1.3 $MgSO_4.7H_2O$, 1.2 KH_2PO_4, 10 HEPES, 25 Glucose, 1 $CaCl_2$, 18.7 $MgCl_2$, osmolarity 300 mOsm/kg H_2O and pH adjusted to 7.4. The spinal cord was included in a 4% low melting point agar in order to glue it in the desired orientation. 300 µm thick lumbar spinal cord slices were obtained following 2 dissecting planes, either transverse or with a 45 degrees angle. The latter orientation was used because we found that the probability of obtaining superficial, and hence easier to patch, ApPrs, was higher. Also, we found that the chances of obtaining "isolated" ApPrs (see Figure 5B) was also higher in the oblique preparation.

Electrophysiological recordings and epifluorescence

CSFcNs were recorded with the patch-clamp technique[44] at near physiological temperature (34 ± 1 °C, Peltier system; Luigs & Neurmann) on an upright Olympus microscope (BX51WI) equipped with a 60×, 1.0 numerical aperture objective. Once in the recording chamber, slices were continuously perfused with the following extracellular solution (in mM): 115 NaCl, 2.5 KCl, 1.3 NaH_2PO_4, 26 $NaHCO_3$, 25 glucose, 5 NaPyruvate, 2 $CaCl_2.2H_2O$ and 1 $MgCl_2.6H_2O$, osmolarity 300 mOsm/kg H_2O and pH 7.4 with the continuous bubbling of a mixture of 95% O_2 and 5% CO_2. Recordings were performed with a KGluconate-based intracellular solution of the following composition (in mM): 165 KGluconate, 10 HEPES, 1 EGTA, 0.1 $CaCl_2$, 4.6 $MgCl_2$, 4 Na_2ATP, 0.4 NaGTP and 0.04 Alexa 594, pH 7.3, and osmolarity 300 mOsm/kg H_2O. With this solution, pipette resistance was 6 to 7 MΩ for somatic and 10 to 11 MΩ for ApPr recordings; series resistance, on the other hand, was monitored during the whole experiment, but not compensated for. Recordings were performed with a HEKA amplifier (EPC10 USB) and the software Patchmaster either in voltage-clamp (-60 mV holding potential) or current-clamp. Recordings were acquired at a sampling rate of 20 kHz and low-pass filtered at 2.9 kHz. Recording and puffing pipettes were positioned in the slice with Luigs & Neumann micromanipulators. Epifluorescence excitation was by light-emitting diodes in a dual lamp-house (Optoled; Cairn Research). EGFP was excited at 470/40 nm and Alexa 594 at 572/35 nm. Fluorescence emission at 520/40 nm and 630/60 nm was detected with an EM CCD camera (Andor Ixon) and filters from Chroma Corporation (Vermont, USA).

Photolysis

Protons were photo-released either from MNI-Glutmate (4-Methoxy-7-nitroindoli-inyl-caged-L-glutamate) or MNI-γLGG (4-Methoxy-7-nitroindoli-inyl-caged-γ-L-glutamyl-glycine) with a 405-nm diode laser (Obis, Coherent, USA) that was focused through the ×60/NA1.0 water immersion objective to a 1.5 µm diameter spot in the sample plane[25,45]. The cages were diluted in the recording ACSF to a final concentration of 0.5 or 1 mM and either pressure-applied with a Picospritzer III (Parker) for at least 10 seconds before applying the light pulses, or bath applied. Photolysis light pulses had durations of 0.5 to 1 ms and 1 to 3 mW laser power. The power of the laser-pulse was monitored on a calibrated photodiode. The laser spot was fixed, and the photolysis location is chosen by positioning the slice on the region of interest. Before each experiment, the exact location of the laser spot was verified by monitoring it with a fluorescent solution.

Salts were either from Sigma-Aldrich or Carlo Erba. TTX (tetrodotoxin; 0.4 µM), TEA (tetraethylammonium; 1.5 mM), 4AP (4 aminopyridine; 1 mM), NBQX (2,3-Dihydroxy-6-nitro-7-sulfamoyl-benzo[f]quinoxaline; 10 µM), D-APV (2-Amino-5-phosphonovaleric acid; 50 µM) and gabazine (10 µM) were from Tocris. MNI-glutamate (1 mM) was from HelloBio and MNI-γLGG (1 mM) was a

generous gift from Dr. Céline Auger (Sppin, CNRS UMR8003). Dibucaine hydrochloride (100 to 200 µM) and calmidazolium chloride (20 µM) were from Sigma-Aldrich. Psalmotoxin 1 (100 nM), APETx2 (100 nM) and TTA-P2 (20 µM) were from Alomone Lab.

Immunohistochemistry

Animals were anesthetized with ketamine (100 mg/kg, i.p.), xylacine (10 mg/kg, i.p.), and diazepam (5 mg/kg, i.p.) and fixed by intracardiac perfusion with 4% PFA in 0.1 M PB. The spinal cord was sectioned with a vibrating microtome (50 - 70 µm thick), placed in PBS with 0.5% BSA for 30 min, and then incubated with the primary mouse anti-PKD2L1 antibody (Millipore-Sigma AB9084, 1:500) in PBS with 0.3% Triton X-100 (Sigma Millipore). Sections were then incubated in the secondary donkey anti-mouse Alexa-647 antibody (Thermo-Fisher A-21235, 1:1000) and mounted in 70% (v/v) glycerol pH 8.8. Nuclei were stained with 1µg/ml Hoechst 33342 (Thermo-Fisher).

Confocal microscopy and image processing

Line selections were manually drawn through either the soma or ApPr of GFP+ cells on single deconvolved confocal planes and fluorescence intensity values per pixel along the selection were obtained using FIJI/ImageJ[46]. Descriptive statistical values were used to build the average and SD plots against position along the selection (x).

Images were acquired on a Zeiss LSM800 confocal microscope with a 63× oil immersion lens (NA = 1.4), pinhole set at 0.8 Airy units. Sampling interval was set to an oversample density according to the Nyquist criterion. Z-stacks were deconvolved with Huygens Essential 4.5 (Scientific Volume Imaging B.V., Hilversum, Netherlands) using an experimental PSF, SNR = 20, using an iterative Classic Maximum Likelihood Estimation (CMLE) algorithm set to a maximum of 40 iterations, with a quality threshold of 0.05. Composite image assembly and further processing (brightness/contrast adjustment), when needed, was performed using FIJI/ImageJ.

Analysis

Electrophysiological analysis was performed with Igor Pro (Wavemetrics) using Neuromatic[47], TaroTools (*https://sites.google.com/site/tarotoolsmember/?authuser=1*) and custom routines. Single-channel currents were analyzed with the software Nest-O-Patch (NOP; *https://sourceforge.net/projects/nestopatch/*). The currents were filtered with the built-in filter of the software (cutt-off filter of 1.4 KHz) and the single-channel current amplitude calculated from a multigaussian fit adjusted to the whole-cell current histogram. Closed and open probabilities were calculated from the idealized current traces. The obtained values were then imported to IgorPro (8.0 or 9.0, Wavemetrics, Lake Oswego) for further analysis.

Current charge was calculated as the integral of the whole-cell recordings after baseline subtraction. Holding current in different conditions was calculated as follows: histograms were constructed from current recordings during 2 to 3 seconds time epochs. Then, the first peak of the resulting histogram, which corresponds to the baseline current, was fitted with a Gaussian function (IgorPro built-in function); the mean value of the fitting corresponds to the tonic current (see Figure 2Bb for an example). In order to show visually the tonic current change in different conditions, current traces were averaged over 100 ms epochs, like what has been done for the analysis of $GABA_A$-mediated tonic currents[48]. For the analysis of resting membrane potential in different conditions, average Vm values were calculated from 1 second long time periods.

Input resistance was measured from the slope of the I/V curve resulting from voltage steps from -110 or 100 to -60 mV in 10 mV increments.

Estimation of the pH drop induced by photolysis

The photolysis of MNI-based compounds leads to proton release. The pH drop induced by the photolysis reaction depends on how many protons are released, on the speed of the buffering system and on the diffusion of molecules in and out of the illuminated volume. In our experiments we used caged-compounds concentrations between 0.5 and 1 mM. Based on our previous

callibrations[25] that indicate that the photolysis is complete with the energy used here (≈ 2 mW for 1 ms), we expect an added charge of 0.5 to 1 mM protons in the illuminated volume, corresponding to a drop of pH from 7.4 to ≈ 3-3.5 pH units. This acid pH is quickly buffered by bicarbonate. Given that the speed of protonation of bicarbonate is extremely fast[49–51], the pH returns to 7.4 within microseconds. This indicates that the late current evoked by the photolysis (Figures 4, **5** and Supplementary Figure 4) has very similar characteristics to the PKD2L1-mediated current that has been described in expression systems in that it is not a delayed current, but rather an off-current that is produced by the opening of the channel when the acidic stimulus is removed. The fact that this off-current is so clearly seen when performing photolysis experiments and not with other methods, like pressure-application, likely reflects the superior temporal resolution of photouncaging. This approach enables exceptionally rapid pH jumps. Similarly, it has been shown by Hu et al[52] that using fast application methods is a necessary condition to induce a type of response, that the authors called Ca^{++} spike, when applying extracellular Ca^{++} stimuli.

Statistics

Data are presented as mean ± SD. Statistical significance was assessed with the Wilcoxon signed-rank test for paired and the Wilcoxon–Mann–Whitney test for non-paired data. The difference between groups was considered significant when $p < 0.05$; when significant, the exact p value is indicated in each figure and figure legends.

Data availability

Numerical data used to make the figures of this manuscript have been deposited at *http://doi.org/10.60895/redata/39X8AV*.

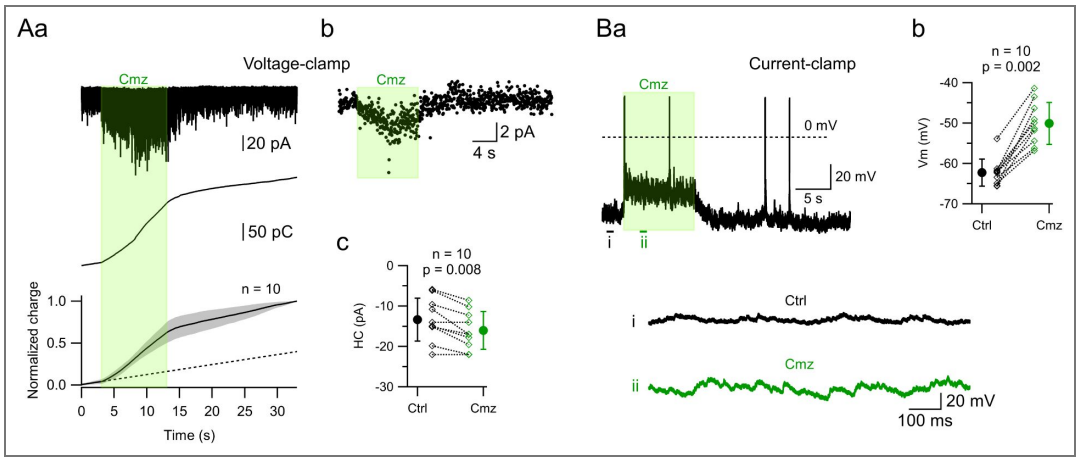

Supplementary Fig. 1. Calmidazolium effect on PKD2L1-mediated tonic and phasic currents. Aa. Top. Spontaneous PKD2L1 channel activity recorded in a CSFcN at a -60 mV holding potential. The recording lasted 35 s, and calmidazolium was pressure-applied at a concentration of 10 µM during 10 s (starting at 3 s, green area). **Middle.** Membrane charge calculated from the recording on the top. **Bottom.** Mean membrane charge ± SD calculated from 10 neurons tested in the same conditions as the cell shown in the top panel. The dotted line corresponds to a linear fit to the control period (first 3 seconds of the recording). The application of calmidazolium produces an increase in the slope of the membrane charge. **Ab.** Holding current from the neuron shown in "**a**". **Ac.** Effect of calmidazolium application on the holding current: -13.3 ± 5.3 pA in control conditions vs -16.0 ± 4.7 pA in calmidazolium (n = 10, p = 0.008). **Ba.** Spontaneous activity of the CSFcN shown in **A**, recorded in current-clamp. Calmidazolium application is indicated with the green area. The bottom traces show segments **i** and **ii** with different time and amplitude scales in order to see the increase in spontaneous activity during calmidazolium. **Bb.** Effect of calmidazolium application on the resting membrane potential. Notice the shift from -62.3 ± 3.3 in control

conditions vs -50.0 ± 5.2 mV in the presence of calmidazolium (n = 10, p = 0.002). In **Ac** and **Bb**, diamonds correspond to individual neurons and circles to the AV ± SD. Cmz: calmidazolium. In **Ac** and **Bb**, statistical comparison between groups was performed with a Wilcoxon signed-rank test.

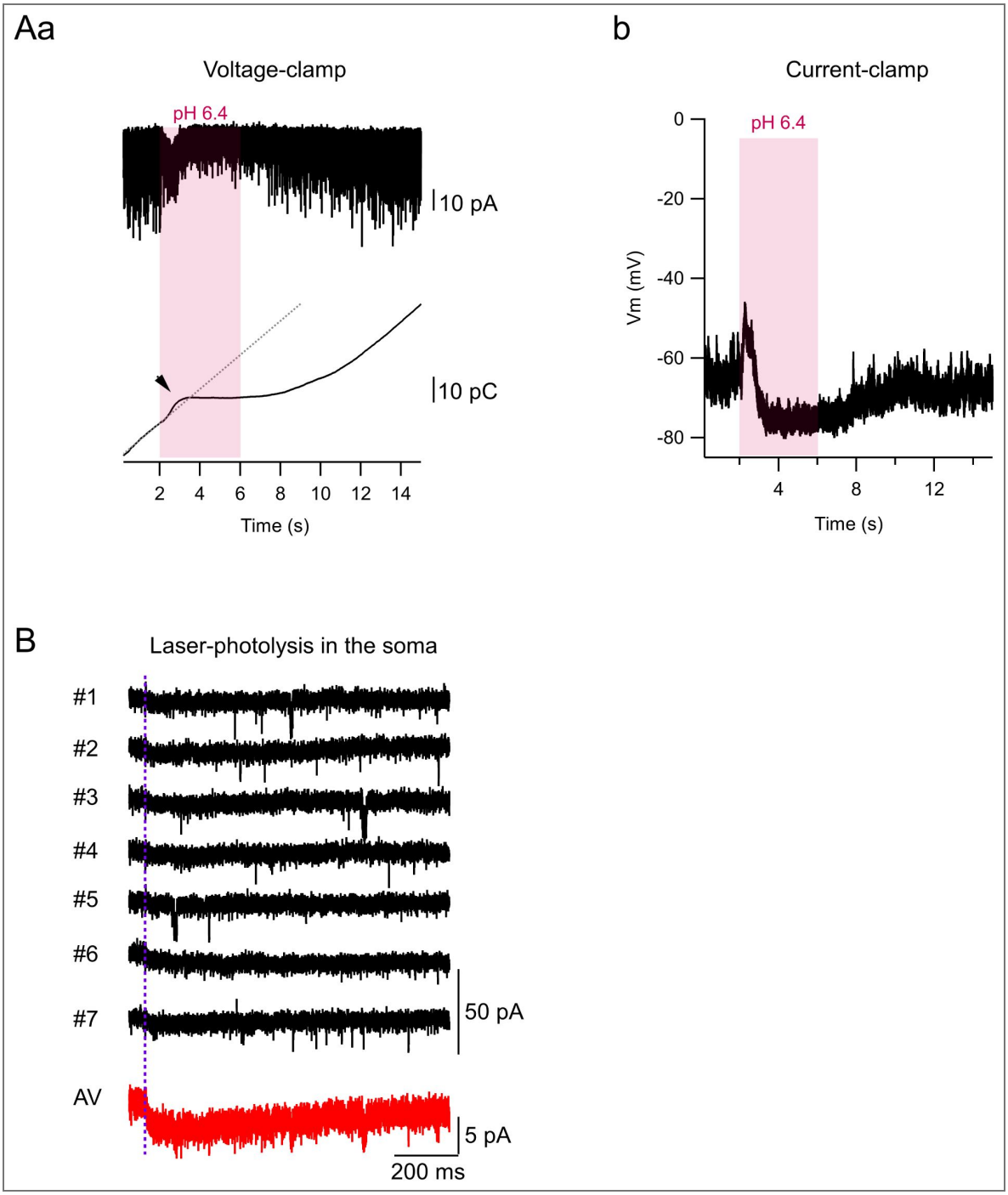

Supplementary Fig. 2. Puffing acidic solutions and proton photolysis in the soma can induce ASIC-mediated currents.

Aa. Top. Spontaneous PKD2L1 channel activity recorded in a CSFcN at a -60 mV holding potential. A pH 6.5 solution was pressure-applied during 4 s (starting at 2 s, magenta area). **Bottom.** Membrane charge calculated from the recording on the top. The dotted line corresponds to a linear fit during the control period (first 2 seconds of the recording). The application of the acidic solution produces a short-lasting inward current that is probably due to the activation of somatic ASIC channels. This is manifested as a sudden increase in the membrane charge (black arrowhead) that is followed by a subsequent decrease. **Ab.** Same experiment as in **a**, under current-clamp. The application of the acidic solution produces a short-lasting depolarization that is probably due to the activation of somatic ASIC channels, followed by hyperpolarization. Vm: membrane potential. **B.** Spontaneous activity recorded in a CSFcN upon the somatic uncaging of MNI-Glutamate. The black traces show individual repetitions (7 uncagings at 10 sec intervals) and the red trace the corresponding average (AV). Vertical dotted magenta line shows the timing of the laser pulse (1 ms, 3 mW). Somatic photolysis does not evoke any PKD2L1-dependent activity, but does produce a small inward current that is probably mediated by ASIC channels.

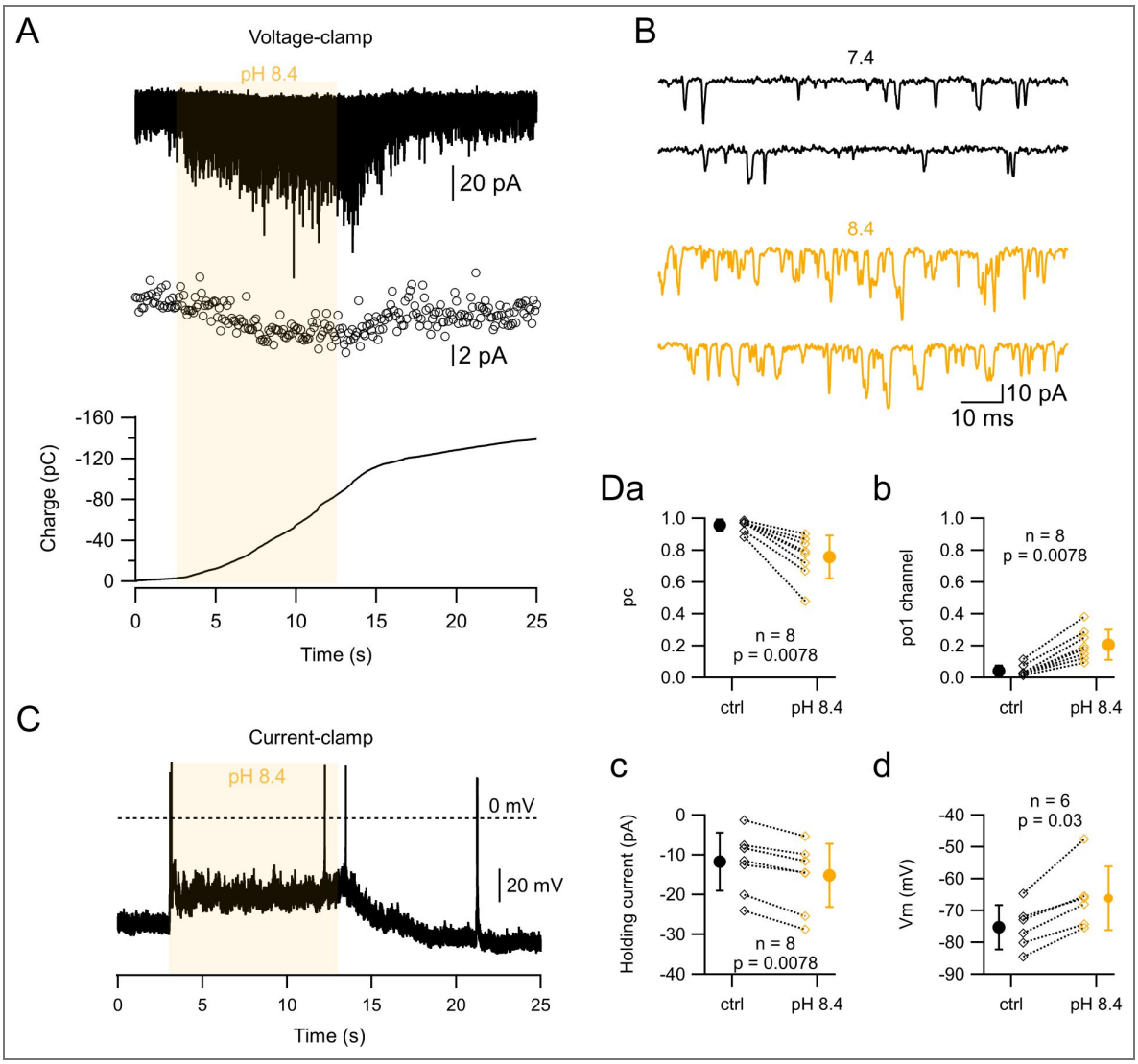

Supplementary Fig. 3. Effect of alkaline ACSF on PKD2L1-mediated currents.

Aa. Top. Spontaneous PKD2L1 channel activity recorded in a CSFcN at a -60 mV holding potential. A pH 8.4 solution was pressure-applied during 10 s (starting at 3 s, yellow area). **Middle.** Holding current calculated from the recording shown on the top. **Bottom.** Membrane charge calculated from the recording shown on the top. **B.** Chosen segments of the recording shown in **A** with different scales. **C.** Same experiment as in **A**, but the spontaneous activity was recorded in current-clamp. The application of the basic solution produces a depolarization of the RMP (from -64.5 to -47.6 mV in this example). **Da.** Effect of the pH 8.4 solution application on the close probability, pc: 0.96 ± 0.036 in control conditions to 0.76 ± 0.13 in the pH 8.4 solution (n = 8, p = 0.0078). **Db.** Effect of the pH 8.4 solution application on po1: 0.042 ± 0.034 in control conditions vs 0.2 ± 0.01 in the pH 8.4 solution (n = 8, p = 0.0078). **Dc.** The application of a pH 8.4 solution produced a shift of the holding current from -11.7 ± 7.3 to -15.2 ± 7.9 pA (n = 8, p = 0.0078). **Dd.** A pH 8.4 solution induced a shift of the resting membrane potential from -75.2 ± 7.0 vs -66.2 ± 10 mV (n = 6, p = 0.03). In **D**, statistical comparison between groups was performed with a Wilcoxon signed-rank test.

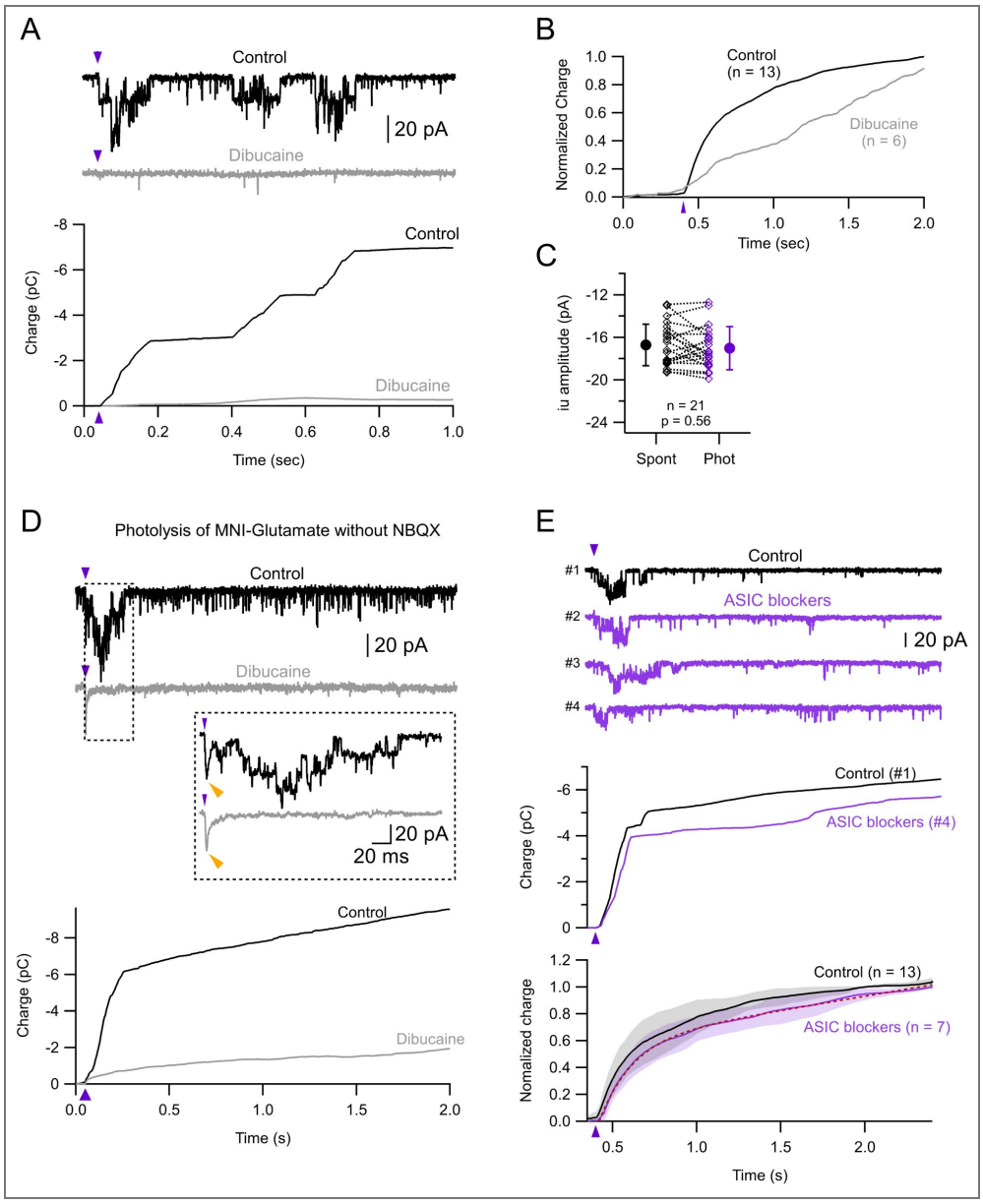

Supplementary Fig. 4. Currents induced by proton photolysis in the ApPr depend on PKD2L1 and not ASIC channels

A. Top. Example of laser-evoked currents in control conditions (black trace) and in the presence of 100 µm dibucaine (gray trace). **Bottom.** Membrane charge calculated from the recordings shown above. **B.** Average, normalized membrane charge calculated from recordings in control conditions (same data as in **4E**) and in the presence of dibucaine. **C.** Single channel current calculated from spontaneous current recordings (spont) and during a 500 ms time window after the photolysis. Gray symbols correspond to individual neurons. Mean ± SD (black symbols): -16.7 ± 2.0 (spont) to 17.0 ± 2.0 (phot) pA, n = 21 neurons, p = 0.56. Wilcoxon signed-rank test. **D. Top.** Example of laser-evoked currents induced by the photolysis of MNI-Glutamate without NBQX (black trace) and without NBQX + dibucaine (gray trace). The inset shows the current traces in expanded scales to better illustrate the AMPA-mediated current (yellow arrowheads). **Bottom.** Membrane charge calculated from the above recordings. **E. Top.** Example of laser-evoked currents induced by the photolysis of MNI-Glutamate without (black trace) and with ASIC channel blockers (magenta traces). **Middle.** Membrane charge calculated from sweeps number 1 (control) and 4 (ASIC blockers). **Bottom.** Normalized (to the 2 s value) membrane charge as a function of time in control conditions (black trace, n = 13; same data as in Figure 4E) and in the presence of ASIC blockers (magenta trace, n = 7). The dotted red line represents the fit to the data with the same function as in Figure 4E. The τ value in the presence of ASIC blockers was 190 ms, close to the 258 ms value for the control curve. Shaded areas represent ± SDs. The magenta arrowheads show the timing of the photolysis pulse. In **C**, statistical comparison between groups was performed with a Wilcoxon signed-rank test.

Acknowledgements

This work was supported by a Agencia Nacional de Investigación e Innovación grant (number FCE_1_2021_1_166464) to Federico F. Trigo and a grant from the Wings For Life Spinal Cord Research Foundation (number WFL-UY-13/23 #290) to Raúl R. Russo. Magdalena Vitar was supported by ANII through a Master Student fellowship. We thank Victoria Falco Pastorino and María Gabriela Fabbiani for their help with the maintenance of the Gata3^{eGFP} colony, Céline Auger for the generous gift of MNI-γLGG, John ET Corrie for initial discussions on the proton photolysis and Alain Marty for the critical reading of the manuscript.

Additional information

Funding

Funder	Grant reference number
Agencia Nacional de Investigación e Innovación	FCE_1_2021_1_166464
Wings For Life Spinal Cord Research Foundation	WFL-UY-13/23 #290

Author ORCID iDs

Daniel Prieto: https://orcid.org/0000-0001-8356-1708

References

(1) **Wyart C.,** Carbo-Tano M., Cantaut-Belarif Y., Orts-Del'Immagine A., Böhm U. L (2023) Cerebrospinal Fluid-Contacting Neurons: Multimodal Cells with Diverse Roles in the CNS. *Nat Rev Neurosci* **24**:540-556 https://doi.org/10.1038/s41583-023-00723-8

(2) **Wang R. L.,** Chang R. B (2024) The Coding Logic of Interoception. *Annual Review of Physiology* **86** https://doi.org/10.1146/annurev-physiol-042222-023455

(3) **Marichal N.,** García G., Radmilovich M., Trujillo-Cenóz O., Russo R. E (2009) Enigmatic Central Canal Contacting Cells: Immature Neurons in "Standby Mode"?. *J. Neurosci* **29**:10010-10024 https://doi.org/10.1523/JNEUROSCI.6183-08.2009

(4) **Orts-Del'Immagine A.,** Kastner A., Tillement V., Tardivel C., Trouslard J., Wanaverbecq N. (2014) Morphology, Distribution and Phenotype of Polycystin Kidney Disease 2-like 1-Positive Cerebrospinal Fluid Contacting Neurons in the Brainstem of Adult Mice. *PLoS One* **9**:e87748 https://doi.org/10.1371/journal.pone.0087748

(5) **Hubbard J. M.,** Böhm U. L., Prendergast A., Tseng P.-E. B., Newman M., Stokes C., Wyart C (2016) Intraspinal Sensory Neurons Provide Powerful Inhibition to Motor Circuits Ensuring Postural Control during Locomotion. *Curr Biol* **26**:2841-2853 https://doi.org/10.1016/j.cub.2016.08.026

(6) **Gerstmann K.,** Jurčić N., Blasco E., Kunz S., de Almeida Sassi F., Wanaverbecq N., Zampieri N (2022) The Role of Intraspinal Sensory Neurons in the Control of Quadrupedal Locomotion. *Curr Biol* **32**:2442-2453.e4. https://doi.org/10.1016/j.cub.2022.04.019

(7) **Nakamura Y.,** Kurabe M., Matsumoto M., Sato T., Miyashita S., Hoshina K., Kamiya Y., Tainaka K., Matsuzawa H., Ohno N., *et al.* (2023) Cerebrospinal Fluid-Contacting Neuron Tracing Reveals Structural and Functional Connectivity for Locomotion in the Mouse Spinal Cord. *eLife* **12**:e83108 https://doi.org/10.7554/eLife.83108

(8) **Fidelin K.,** Djenoune L., Stokes C., Prendergast A., Gomez J., Baradel A., Del Bene F., Wyart C (2015) State-Dependent Modulation of Locomotion by GABAergic Spinal Sensory Neurons. *Curr Biol* **25**:3035-3047 https://doi.org/10.1016/j.cub.2015.09.070

(9) **Wu M.-Y.,** Carbó-Tano M., Mirat O., Lejeune F.-X., Roussel J., Quan F., Fidelin K., Wyart C (2021) Spinal Sensory Neurons Project onto Hindbrain to Stabilize Posture and Enhance Locomotor Speed. *bioRxiv* https://doi.org/10.1101/2021.03.16.435696

(10) **Jalalvand E.,** Robertson B., Wallén P., Grillner S (2016) Ciliated Neurons Lining the Central Canal Sense Both Fluid Movement and pH through ASIC3. *Nat Commun* **7** https://doi.org/10.1038/ncomms10002

(11) **DeCaen P. G.,** Delling M., Vien T. N., Clapham D. E (2013) Direct Recording and Molecular Identification of the Calcium Channel of Primary Cilia. *Nature* **504**:315-318 https://doi.org/10.1038/nature12832

(12) **Huang A. L.,** Chen X., Hoon M. A., Chandrashekar J., Guo W., Tränkner D., Ryba N. J. P., Zuker C. S (2006) The Cells and Logic for Mammalian Sour Taste Detection. *Nature* **442**:934-938 https://doi.org/10.1038/nature05084

(13) **Jalalvand E.,** Robertson B., Tostivint H., Wallén P., Grillner S (2016) The Spinal Cord Has an Intrinsic System for the Control of pH. *Curr. Biol* **26**:1346-1351 https://doi.org/10.1016/j.cub.2016.03.048

(14) **Orts-Del'immagine A.,** Wanaverbecq N., Tardivel C., Tillement V., Dallaporta M., Trouslard J (2012) Properties of Subependymal Cerebrospinal Fluid Contacting Neurones in the Dorsal Vagal Complex of the Mouse Brainstem. *J. Physiol. (Lond.)* **590**:3719-3741 https://doi.org/10.1113/jphysiol.2012.227959

(15) **Orts-Del'Immagine A.,** Seddik R., Tell F., Airault C., Er-Raoui G., Najimi M., Trouslard J., Wanaverbecq N (2016) A Single Polycystic Kidney Disease 2-like 1 Channel Opening Acts as a Spike Generator in Cerebrospinal Fluid-Contacting Neurons of Adult Mouse Brainstem. *Neuropharmacology* **101**:549-565 https://doi.org/10.1016/j.neuropharm.2015.07.030

(16) **Panayi H.,** Panayiotou E., Orford M., Genethliou N., Mean R., Lapathitis G., Li S., Xiang M., Kessaris N., Richardson W. D., *et al.* (2010) Sox1 Is Required for the Specification of a Novel P2-Derived Interneuron Subtype in the Mouse Ventral Spinal Cord. *J. Neurosci* **30**:12274-12280 https://doi.org/10.1523/JNEUROSCI.2402-10.2010

(17) **Petracca Y. L.,** Sartoretti M. M., Di Bella D. J., Marin-Burgin A., Carcagno A. L., Schinder A. F., Lanuza G. M (2016) The Late and Dual Origin of Cerebrospinal Fluid-Contacting Neurons in the Mouse Spinal Cord. *Development* **143**:880-891 https://doi.org/10.1242/dev.129254

(18) **Sternberg J. R.,** Prendergast A. E., Brosse L., Cantaut-Belarif Y., Thouvenin O., Orts-Del'Immagine A., Castillo L., Djenoune L., Kurisu S., McDearmid J. R., *et al.* (2018) Pkd2l1 Is Required for Mechanoception in Cerebrospinal Fluid-Contacting Neurons and Maintenance of Spine Curvature. *Nat Commun* **9**:3804 https://doi.org/10.1038/s41467-018-06225-x

(19) **DeCaen P. G.,** Liu X., Abiria S., Clapham D. E (2016) Atypical Calcium Regulation of the PKD2-L1 Polycystin Ion Channel. *eLife* **5**:e13413 https://doi.org/10.7554/eLife.13413

(20) **Guadarrama E.,** Vanoye C. G., DeCaen P. G (2025) Defining the Polycystin Pharmacophore Through HTS & Computational Biophysics. *bioRxiv* https://doi.org/10.1101/2025.01.13.632808

(21) **Russo R. E.,** Fernández A., Reali C., Radmilovich M., Trujillo-Cenóz O (2004) Functional and Molecular Clues Reveal Precursor-like Cells and Immature Neurones in the Turtle Spinal Cord. *J Physiol* **560**:831-838 https://doi.org/10.1113/jphysiol.2004.072405

(22) **Park E. Y. J.,** Baik J. Y., Kwak M., So I (2019) The Role of Calmodulin in Regulating Calcium-Permeable PKD2L1 Channel Activity. *Korean J Physiol Pharmacol* **23**:219-227 https://doi.org/10.4196/kjpp.2019.23.3.219

(23) **González-Perrett S.,** Batelli M., Kim K., Essafi M., Timpanaro G., Moltabetti N., Reisin I. L., Arnaout M. A., Cantiello H. F (2002) Voltage Dependence and pH Regulation of Human Polycystin-2-Mediated Cation Channel Activity *. *Journal of Biological Chemistry* **277**:24959-24966 https://doi.org/10.1074/jbc.M105084200

(24) **Chen P.,** Wu J., Zhao J., Wang P., Luo J., Yang W., Liu X (2015) PKD2L1/PKD1L3 Channel Complex with an Alkali-Activated Mechanism and Calcium-Dependent Inactivation. *Eur Biophys J* **44**:483-492 https://doi.org/10.1007/s00249-015-1040-y

(25) **Trigo F. F.,** Corrie J. E. T., Ogden D (2009) Laser Photolysis of Caged Compounds at 405 Nm: Photochemical Advantages, Localisation, Phototoxicity and Methods for Calibration. *Journal of Neuroscience Methods* **180**:9-21 https://doi.org/10.1016/j.jneumeth.2009.01.032

(26) **Blanchard K,** Zorrilla de San Martín J., Marty A., Llano I., Trigo F. F. (2020) Differentially Poised Vesicles Underlie Fast and Slow Components of Release at Single Synapses. *J. Gen. Physiol* **152** https://doi.org/10.1085/jgp.201912523

(27) **Canepari M.,** Nelson L., Papageorgiou G., Corrie J. E. T., Ogden D (2001) Photochemical and Pharmacological Evaluation of 7-Nitroindolinyl-and 4-Methoxy-7-Nitroindolinyl-Amino Acids as Novel, Fast Caged Neurotransmitters. *Journal of Neuroscience Methods* **112**:29-42 https://doi.org/10.1016/S0165-0270(01)00451-4

(28) **Palma-Cerda F.,** Papageorgiou G., Barbour B., Auger C., Ogden D (2018) Photolysis of a Caged, Fast-Equilibrating Glutamate Receptor Antagonist, MNI-Caged γ-D-Glutamyl-Glycine, to Investigate Transmitter Dynamics and Receptor Properties at Glutamatergic Synapses. *Front Cell Neurosci* **12** https://doi.org/10.3389/fncel.2018.00465

(29) **Hussein S.,** Zheng W., Dyte C., Wang Q., Yang J., Zhang F., Tang J., Cao Y., Chen X.-Z (2015) Acid-Induced off-Response of PKD2L1 Channel in Xenopus Oocytes and Its Regulation by Ca2+. *Sci Rep* **5** https://doi.org/10.1038/srep15752

(30) **Inada H.,** Kawabata F., Ishimaru Y., Fushiki T., Matsunami H., Tominaga M (2008) Off-response Property of an Acid-activated Cation Channel Complex PKD1L3–PKD2L1. *EMBO reports* **9**:690-697 https://doi.org/10.1038/embor.2008.89

(31) **Jalalvand E.,** Robertson B., Tostivint H., Löw P., Wallén P., Grillner S (2018) Cerebrospinal Fluid-Contacting Neurons Sense pH Changes and Motion in the Hypothalamus. *J. Neurosci* **38**:7713-7724 https://doi.org/10.1523/JNEUROSCI.3359-17.2018

(32) **Rook M. L.,** Musgaard M., MacLean D. M (2021) Coupling Structure with Function in Acid-Sensing Ion Channels: Challenges in Pursuit of Proton Sensors. *J Physiol* **599**:417-430 https://doi.org/10.1113/JP278707

(33) **Djenoune L.,** Khabou H., Joubert F., Quan F. B., Nunes Figueiredo S., Bodineau L., Del Bene F., Burcklé C., Tostivint H., Wyart C (2014) Investigation of Spinal Cerebrospinal Fluid-Contacting Neurons Expressing PKD2L1: Evidence for a Conserved System from Fish to Primates. *Front. Neuroanat* **8** https://doi.org/10.3389/fnana.2014.00026

(34) **Bruni J. E.,** Reddy K (1987) Ependyma of the Central Canal of the Rat Spinal Cord: A Light and Transmission Electron Microscopic Study. *J Anat* **152**:55-70

(35) **Bjugn R.,** Haugland H. K., Flood P. R (1988) Ultrastructure of the Mouse Spinal Cord Ependyma. *J Anat* **160**:117-125

(36) **Lyckenvik T.,** Forsberg M., Johansson K., Axelsson M., Zetterberg H., Blennow K., Illes S., Wasling P., Hanse E (2025) Ion Concentrations in CSF and Serum Are Differentially and Precisely Regulated. *Brain Communications* **7**:fcaf201 https://doi.org/10.1093/braincomms/fcaf201

(37) **Uchitel O. D.,** González Inchauspe C., Weissmann C (2019) Synaptic Signals Mediated by Protons and Acid-Sensing Ion Channels. *Synapse* **73**:e22120 https://doi.org/10.1002/syn.22120

(38) **Clements JD,** Lester RA, Tong G, Jahr CE, Westbrook GL (1992) The time course of glutamate in the synaptic cleft. *Science* **258**:1498-501 https://doi.org/10.1126/science.1359647

(39) **Brickley S. G.,** Cull-Candy S. G., Farrant M (1996) Development of a Tonic Form of Synaptic Inhibition in Rat Cerebellar Granule Cells Resulting from Persistent Activation of GABAA Receptors. *J Physiol* **497** https://doi.org/10.1113/jphysiol.1996.sp021806

(40) **Kawaguchi H.,** Yamanaka A., Uchida K., Shibasaki K., Sokabe T., Maruyama Y., Yanagawa Y., Murakami S., Tominaga M (2010) Activation of Polycystic Kidney Disease-2-like 1 (PKD2L1)-PKD1L3 Complex by Acid in Mouse Taste Cells. *J Biol Chem* **285**:17277-17281 https://doi.org/10.1074/jbc.C110.132944

(41) **Prendergast A. E.,** Jim K. K., Marnas H., Desban L., Quan F. B., Djenoune L., Laghi V., Hocquemiller A., Lunsford E. T., Roussel J., *et al.* (2023) CSF-Contacting Neurons Respond to Streptococcus Pneumoniae and Promote Host Survival during Central Nervous System Infection. *Current Biology* **33**:940-956.e10. https://doi.org/10.1016/j.cub.2023.01.039

(42) **Cristofori-Armstrong B.,** Rash L. D (2017) Acid-Sensing Ion Channel (ASIC) Structure and Function: Insights from Spider, Snake and Sea Anemone Venoms. *Neuropharmacology* **127**:173-184 https://doi.org/10.1016/j.neuropharm.2017.04.042

(43) **Zhang Y.,** Muyrers J. P., Testa G., Stewart A. F (2000) DNA Cloning by Homologous Recombination in Escherichia Coli. *Nat Biotechnol* **18**:1314-1317 https://doi.org/10.1038/82449

(44) **Hamill O. P.,** Marty A., Neher E., Sakmann B., Sigworth F. J (1981) Improved Patch-Clamp Techniques for High-Resolution Current Recording from Cells and Cell-Free Membrane Patches. *Pflugers Arch* **391**:85-100

(45) **Zorrilla de San Martin J.,** Jalil A., Trigo F. F. (2015) Impact of Single-Site Axonal GABAergic Synaptic Events on Cerebellar Interneuron Activity. *J. Gen. Physiol* **146**:477-493 https://doi.org/10.1085/jgp.201511506

(46) **Schindelin J.,** Arganda-Carreras I., Frise E., Kaynig V., Longair M., Pietzsch T., Preibisch S., Rueden C., Saalfeld S., Schmid B., *et al.* (2012) Fiji: An Open-Source Platform for Biological-Image Analysis. *Nat Methods* **9**:676-682 https://doi.org/10.1038/nmeth.2019

(47) **Rothman J. S.,** Silver R. A (2018) NeuroMatic: An Integrated Open-Source Software Toolkit for Acquisition, Analysis and Simulation of Electrophysiological Data. *Front. Neuroinform* **12** https://doi.org/10.3389/fninf.2018.00014

(48) **Bright D.,** Smart T. G (2013) Methods for Recording and Measuring Tonic GABAA Receptor-Mediated Inhibition. *Front. Neural Circuits* **7** https://doi.org/10.3389/fncir.2013.00193

(49) **Gibbons B. H.,** Edsall J. T (1963) Rate of hydration of carbon dioxide and dehydration of carbonic acid at 25 degrees. *J Biol Chem* **238**:3502-3507

(50) **Ho C.,** Sturtevant J. M (1963) The kinetics of the hydration of carbon dioxide at 25 degrees. *J Biol Chem* **238**:3499-3501

(51) **Eigen M.** (1964) Proton Transfer, Acid-Base Catalysis, and Enzymatic Hydrolysis. Part I: ELEMENTARY PROCESSES. *Angewandte Chemie International Edition in English* **3**:1-19 https://doi.org/10.1002/anie.196400011

(52) **Hu M.,** Liu Y., Wu J., Liu X (2015) Influx-Operated Ca2+ Entry via PKD2-L1 and PKD1-L3 Channels Facilitates Sensory Responses to Polymodal Transient Stimuli. *Cell Reports* **13**:798-811 https://doi.org/10.1016/j.celrep.2015.09.041

Peer reviews

Reviewer #1 (Public review):

This study by Vitar et al. probes the molecular identity and functional specialization of pH-sensing channels in cerebrospinal fluid-contacting neurons (CSFcNs). Combining patch-clamp electrophysiology, laser-based local acidification, immunohistochemistry, and confocal imaging, the authors propose that PKD2L1 channels localized to the apical protrusion (ApPr) function as the predominant dual-mode pH sensor in these cells.

The work establishes a compelling spatial-physiological link between channel localization and chemosensory behavior. The integration of optical and electrical approaches is technically strong, and the separation of phasic and sustained response modes offers a useful conceptual advance for understanding how CSF composition is monitored.

Several aspects of data interpretation, however, require clarification or reanalysis-most notably the single-channel analyses (event counts, Po metrics, and mixed parameters), the

statistical treatment, and the interpretation of purported "OFF currents." Additional issues include PKD2L1-TRPP3 nomenclature consistency, kinetic comparison with ASICs, and the physiological relevance of the extreme acidification paradigm. Addressing these points will substantially improve reproducibility and mechanistic depth.

Overall, this is a scientifically important and technically sophisticated study that advances our understanding of CSF sensing, provided that the analytical and interpretative weaknesses are satisfactorily corrected.

(1) The authors should re-analyze electrophysiological data, focusing on macroscopic currents rather than statistically unreliable Po calculations. Remove or revise the Po analysis, which currently conflates current amplitude and open probability.

(2) PKD2L1-TRPP3 nomenclature should be clarified and all figure labels, legends, and text should use consistent terminology throughout.

(3) The authors should reinterpret the so-called OFF currents as pH-dependent recovery or relaxation phenomena, not as distinct current species. Remove the term "OFF response" from the manuscript.

(4) Evidence for physiological relevance should be provided, including data from milder acidification (pH 6.5-6.8) and, where appropriate, comparisons with ASIC-mediated currents to place PKD2L1 activity in context.

(5) Terminology and data presentation should be unified, adopting consistent use of "predominant" (instead of "exclusive") and "sustained" (instead of "tonic"), and all statistical formats and units should be standardized.

(6) The Discussion should be expanded to address potential Ca^{2+}-dependent signaling mechanisms downstream of PKD2L1 activation and their possible roles in CSF flow regulation and central chemoreception.

https://doi.org/10.7554/eLife.109372.1.sa2

Reviewer #2 (Public review):

Summary:

Cerebrospinal fluid contacting neurons (CSF-cNs) are GABAergic cells surrounding the spinal cord central canal (CC). In mammals, their soma lies sub-ependymally, with a dendritic-like apical extension (AP) terminating as a bulb inside the CC.

How this anatomy-soma and AP in distinct extracellular environments relate to their multimodal CSF-sensing function remains unclear.

The authors confirm that in GATA3:GFP mice, where these cells are labeled, that CSFcNs exhibit prominent spontaneous electrical activity mediated by PKD2L1 (TRPP2) channels, non-selective cation channels with ~200 pS conductance modulated by protons and mechanical forces.

They investigated PKD2L1 pH sensitivity and its effects on CSFcN excitability. They uncovered that PKD2L1 generates both phasic and tonic currents, bidirectionally modulated by pH with high sensitivity near physiological values.

Combining electrophysiology (intact and isolated AP recordings) with elegant laser-photolysis, they show that functional PKD2L1 channels localize specifically to the apical extension (AP).

This spatial segregation, coupled with PKD2L1's biophysical properties (high conductance, pH sensitivity) and the AP's unique features (very high input resistance), renders CSFcN excitability highly sensitive to PKD2L1 modulation. Their findings reveal how the AP's properties are optimised for its sensory role.

Strengths:

This is a very convincing demonstration using elegant and challenging approaches (uncaging, outside out patch of the AP) together to form a complete understanding of how these sensory cells can detect the changes of pH in the CSF so finely.

Weaknesses:

The following do not constitute weaknesses; rather, they are minor requests that this reviewer considers would complete this beautiful study.

(1) It would be nice to quantify further the relation in spontaneous as well as in acidic or basic pH between the effects observed on channel opening and holding current: do they always vary together and in a linear way?

(2) Since CSF-cNs also respond to changes in osmolarity (Orts Dell Immagine 2013) & mechanosensory stimulations in a PKD2L1 dependent manner (Sternberg NC 2018), it would be nice to test the same results whether the same results hold true on the role of PKD2L1 in AP for pressure application of changes in osmolarity.

In mice, like in fish (Sternberg et al, NC 2018), we can observe throughout the figures that a large fraction of the channel activity occurs with partial and very fast openings of the PKD2L1 channel. I recommend the authors analyse the points below:

a) To what extent do these partial openings of the channel contribute to the changes in holding current and resting potential?

b) In the trace from the outside out AP, it looks like the partial transient openings are gone. Can the authors verify whether these partial openings are only present in somatic recordings?

(3) Previous studies have observed expression of metabotropic Glutamate receptors in CSF-cNs (transcriptome from Prendergast et al CB 2023). The authors only used blockers for ionotropic glutamate receptors in their recordings: could it be that these metabotropic receptors influence the response to uncaging of MNI-Glu when glutamate is co-released with a proton?

(4) In the outside out patch of the AP, PKD2L1 unitary currents appear rare. Could it be that the disruption in the cilium or underlying actin/myosin cytoskeleton drastically alter the open probability of the channel?

(5) Could the authors use drugs against ASIC to specify which ASIC channels contribute to the pH response in the soma?

(6) This is out of the scope of this study, but we did observe in fish a very rarely-opening channel in the PKD2L1KO mutant. I wonder if the authors have similar observations in the conditions where PKD2L1 is mainly in the closed state.

https://doi.org/10.7554/eLife.109372.1.sa1

Author response:

Public Reviews:

Reviewer #1 (Public review):

This study by Vitar et al. probes the molecular identity and functional specialization of pH-sensing channels in cerebrospinal fluid-contacting neurons (CSFcNs). Combining patch-clamp electrophysiology, laser-based local acidification, immunohistochemistry, and confocal imaging, the authors propose that PKD2L1 channels localized to the apical protrusion (ApPr) function as the predominant dual-mode pH sensor in these cells.

The work establishes a compelling spatial-physiological link between channel localization and chemosensory behavior. The integration of optical and electrical approaches is technically strong, and the separation of phasic and sustained response modes offers a useful conceptual advance for understanding how CSF composition is monitored.

Several aspects of data interpretation, however, require clarification or reanalysis-most notably the single-channel analyses (event counts, Po metrics, and mixed parameters), the statistical treatment, and the interpretation of purported "OFF currents." Additional issues include PKD2L1-TRPP3 nomenclature consistency, kinetic comparison with ASICs, and the physiological relevance of the extreme acidification paradigm. Addressing these points will substantially improve reproducibility and mechanistic depth.

Overall, this is a scientifically important and technically sophisticated study that advances our understanding of CSF sensing, provided that the analytical and interpretative weaknesses are satisfactorily corrected.

(1) The authors should re-analyze electrophysiological data, focusing on macroscopic currents rather than statistically unreliable Po calculations. Remove or revise the Po analysis, which currently conflates current amplitude and open probability.

We agree with the reviewer that the Po analysis has strong limitations, particularly in experiments where the recording times are short, such as when extracellular pH is changed via photolysis (Figure 4D) or puff application (Figure 3Aa). To circumvent this problem and not rely solely on Po estimations, we used alternative methods, including an analysis of the total membrane charge (extensively used throughout the manuscript, as in Figures 3A and 4D) and an analysis of event latencies (Figure 4G). Nevertheless, single channel recordings contain information that is not included in the macroscopic current analysis. In the revised version, we intend to stress that the elementary current amplitude is conserved during manipulations such as pH changes, leaving the total number of channels (N) and the channel open probability (Po) as possible culprits for the current changes. Since these changes are rapid and reversible, it is likely that N remains constant while Po changes. To address the reviewer's concern, we propose the following changes/reanalysis: (i) report in each condition the minimum N (based on the maximum number of simultaneously open channels; for example, in Figure 3Aa, the minimum N goes from 4-5 in control conditions to 1 during the puff of the pH 6.4 solution). Although imperfect, this method provides a tentative estimate of Po; (ii) report the fraction of time that the channels remain open; (iii) revise the text and figures to use the expression "apparent Po" instead of "Po", acknowledging the limitations of the measurement in short recordings. We also acknowledge that some traces (Figure 3Aa, top) may appear confusing, as they seem to show macroscopic currents. We will modify these figures by including the amplitude histograms (as in Figure 1Bb) to clearly demonstrate that recordings from CSFcNs primarily reflect single-channel activity when challenged with pH changes.

> *(2) PKD2L1-TRPP3 nomenclature should be clarified and all figure labels, legends, and text should use consistent terminology throughout.*

We agree with the reviewer that the nomenclature for the polycystin protein family is confusing. In this manuscript, we have followed the nomenclature proposed in a recent comprehensive review on polycystin channels by Palomero, Larmore and DeCaen (Palomero et al. 2023), which refer to the channels by their gene names. As indicated in that review, the PKD2L1 channel corresponds to TRPP2 (previously known as TRPP3, see their Table 1). However, in another recent review on TRP channels, the PKD2L1 channel is referred to as TRPP3 (Zhang et al. 2023). To prevent any ambiguity, we will remove references to the TRPP nomenclature from the text and exclusively use the PKD2L1 acronym.

> *(3) The authors should reinterpret the so-called OFF currents as pH-dependent recovery or relaxation phenomena, not as distinct current species. Remove the term "OFF response" from the manuscript.*

Although largely used in the literature, we concur with the reviewer that the term “OFF response” is not very helpful from a biophysical perspective as it may imply the existence of a distinct current. Consequently, we will remove the terms “OFF response” and “OFF current” from the revised manuscript and replace them with the term “photolysis-evoked PKD2L1 current”. Furthermore, to improve the logical flow, we will condense the two sections (“The proton-induced current is an off-current” and “The off-current is mediated by the activation of PKD2L1 channels”) into a single, new section titled “The photolysis-induced current is mediated by PKD2L1 channels”. This consolidation will prevent the artificial separation of the description of this current. Finally, we will revise the discussion to better characterize this photolysis-evoked phenomenon as a recovery current.

> *(4) Evidence for physiological relevance should be provided, including data from milder acidification (pH 6.5-6.8) and, where appropriate, comparisons with ASIC-mediated currents to place PKD2L1 activity in context.*

This point is partly addressed in Figure 3. The data indicate that PKD2L1 channels are highly sensitive to pH variations within the physiological range. To strengthen this conclusion, we will add the EC50 values derived from the curve fittings to the figure. Regarding ASIC-mediated currents, one of our main conclusions is that ASICs are not present in the apical process (ApPr), as the effects of proton photolysis in the ApPr are not blocked by ASIC antagonists. Our results suggest that PKD2L1 channels are the exclusive pH sensitive channels in the ApPr. ASIC channels likely mediate acid sensitivity in the soma, although we have not investigated the latter in detail. We intend to modify the Discussion in order to provide a physiological framework linking channel activity with physiological and pathophysiological pH changes.

> *(5) Terminology and data presentation should be unified, adopting consistent use of "predominant" (instead of "exclusive") and "sustained" (instead of "tonic"), and all statistical formats and units should be standardized.*

Folllowing the reviewer’s suggestions, an exhaustive rephrasing will be performed to unify terminology, data presentation and correct the text.

> *(6) The Discussion should be expanded to address potential Ca^{2+}-dependent signaling mechanisms downstream of PKD2L1 activation and their possible roles in CSF flow regulation and central chemoreception.*

This is indeed a very interesting and currently unresolved point in the physiology of CSFcNs. Published data indicate that calcium influx through PKD2L1 channels is a key regulator of apical process (ApPr) physiology. These channels are calcium permeable yet are also

inhibited by intracellular calcium (DeCaen et al. 2016). Additionally, ultrastructural data show that the ApPr is rich in mitochondria and tubulo-vesicular structures resembling the Golgi apparatus (Bruni et Reddy 1987; Bjugn et al. 1988; Nakamura et al. 2023), intracellular organelles critical for calcium homeostasis. Altogether, this evidence suggests that intra-ApPr calcium concentration must be finely regulated, both in space and time, for the ApPr to fulfill its physiological roles. Based on the existing literature, we can speculate that these calcium signals are decoded by several systems: (i) calcium may act as a second messenger, linking the activation of the multimodal PKD2L1 channels to changes in CSFcN excitability, which in turn regulates spinal neuronal networks controlling locomotor activity; (ii) calcium could initiate the neurosecretion of various molecules from the ApPr into the central canal, as proposed by the Wyart group in the zebrafish in the context of bacterial infections (Prendergast et al. 2023); (iii) calcium could activate the Hedgehog signaling pathway (as has been shown by Delling et al. 2013); iv) calcium could modulate CSF flow by modulating ependymal cells ciliary activity. Resolving these downstream pathways is essential to fully define the role of CSFcNs as integrators of cerebrospinal fluid homeostasis. We will expand on this topic in the Discussion section of the revised ms.

> ***Reviewer #2 (Public review):***
>
> *Summary:*
>
> *Cerebrospinal fluid contacting neurons (CSF-cNs) are GABAergic cells surrounding the spinal cord central canal (CC). In mammals, their soma lies sub-ependymally, with a dendritic-like apical extension (AP) terminating as a bulb inside the CC.*
>
> *How this anatomy-soma and AP in distinct extracellular environments relate to their multimodal CSF-sensing function remains unclear.*
>
> *The authors confirm that in GATA3:GFP mice, where these cells are labeled, that CSFcNs exhibit prominent spontaneous electrical activity mediated by PKD2L1 (TRPP2) channels, non-selective cation channels with ~200 pS conductance modulated by protons and mechanical forces.*
>
> *They investigated PKD2L1 pH sensitivity and its effects on CSFcN excitability. They uncovered that PKD2L1 generates both phasic and tonic currents, bidirectionally modulated by pH with high sensitivity near physiological values.*
>
> *Combining electrophysiology (intact and isolated AP recordings) with elegant laser-photolysis, they show that functional PKD2L1 channels localize specifically to the apical extension (AP).*
>
> *This spatial segregation, coupled with PKD2L1's biophysical properties (high conductance, pH sensitivity) and the AP's unique features (very high input resistance), renders CSFcN excitability highly sensitive to PKD2L1 modulation. Their findings reveal how the AP's properties are optimised for its sensory role.*
>
> *Strengths:*
>
> *This is a very convincing demonstration using elegant and challenging approaches (uncaging, outside out patch of the AP) together to form a complete understanding of how these sensory cells can detect the changes of pH in the CSF so finely.*
>
> *Weaknesses:*
>
> *The following do not constitute weaknesses; rather, they are minor requests that this reviewer considers would complete this beautiful study.*

> *(1) It would be nice to quantify further the relation in spontaneous as well as in acidic or basic pH between the effects observed on channel opening and holding current: do they always vary together and in a linear way?*

Following the reviewer's suggestion, we performed a Spearman's rank correlation test. The analysis revealed a significant correlation between the changes in the apparent open probability and the holding current in paired experiments (control vs pH 6.4 pressure applications; $p < 0.05$, Spearman $r = 0.72$ and critical value = 0.67). The Pearson correlation coefficient calculated on the same data set was $r = 0.63$ (critical value = 0.632), indicating that the correlation is not linear. We thank the reviewer for raising this point and will add this analysis to the manuscript.

> *(2) Since CSF-cNs also respond to changes in osmolarity (Orts Dell Immagine 2013) & mechanosensory stimulations in a PKD2L1 dependent manner (Sternberg NC 2018), it would be nice to test the same results whether the same results hold true on the role of PKD2L1 in AP for pressure application of changes in osmolarity.*

This is a very important point. As the reviewer notes, previous experimental evidence indicates that CSFcNs are also sensitive to osmolarity changes and mechanical stimulation in a PKD2L1-dependent manner. It is therefore reasonable to assume that, similar to pH sensitivity, osmotic and mechanical sensitivity depend on channels localized to the apical process (ApPr). Regarding mechanosensitivity, this spatial segregation could be tested by mechanically stimulating either the ApPr or the soma with a piezo-controlled blunt pipette (see, for example, Hao et al. 2013). Assessing sensitivity to osmotic changes, however, is more challenging, as pressure application lacks the spatial resolution to discriminate between compartments in such a compact cell. In theory, a highly localized osmotic jump could be achieved via photolysis, provided a caged compound that releases many osmotic particles simultaneously is used. In typical photolysis experiments, a localized osmotic change is produced, but its amplitude is very low (on the order of 1 to 2 mOsm).

> *In mice, like in fish (Sternberg et al, NC 2018), we can observe throughout the figures that a large fraction of the channel activity occurs with partial and very fast openings of the PKD2L1 channel. I recommend the authors analyse the points below:*
>
> *(a) To what extent do these partial openings of the channel contribute to the changes in holding current and resting potential?*

As the reviewer indicates, these partial and rapid openings are characteristic of PKD2L1 single-channel activity and appear to be conserved across species. However, estimating their precise contribution to the sustained current would require a detailed channel model, which is currently lacking. Indeed, the exact mechanism underlying this prominent sustained current in CSFcNs remains unknown and should definitely be addressed in future work.

> *(b) In the trace from the outside out AP, it looks like the partial transient openings are gone. Can the authors verify whether these partial openings are only present in somatic recordings?*

The outside-out recordings from the apical process also show some partial openings (see the upper trace in Figure 4Db). We will specifically mention this important point in the revised version of the ms.

> *(3) Previous studies have observed expression of metabotropic Glutamate receptors in CSF-cNs (transcriptome from Prendergast et al CB 2023). The authors only used blockers for ionotropic glutamate receptors in their recordings: could it be that these metabotropic receptors influence the response to uncaging of MNI-Glu when glutamate is co-released with a proton?*

We thank the reviewer for pointing out the presence of metabotropic glutamate receptors in CSFcNs. However, our evidence indicates that metabotropic receptors do not contribute to the response when uncaging MNI-glutamate. This conclusion is supported by two observations: (i) the response obtained when uncaging MNI-γLGG, which does not release glutamate (Figure 5Ab), and (ii) the response obtained when uncaging protons from DPNI-GABA (data not shown) (DPNI-GABA is a GABA cage with photochemistry similar to MNI cages that also releases a proton upon photolysis; Trigo et al. 2009), are the same. In both experiments (uncaging MNI-γLGG or DPNI-GABA) a clear photolysis-evoked PKD2L1 current is observed.

> *(4) In the outside out patch of the AP, PKD2L1 unitary currents appear rare. Could it be that the disruption in the cilium or underlying actin/myosin cytoskeleton drastically alter the open probability of the channel?*

The reviewer is correct in noting that the opening frequency of PKD2L1 channels appears lower in outside-out patches than in whole-ApPr recordings, although we have not quantified this. We interpreted this difference as reflecting a lower channel number. However, as the reviewer suggests, a plausible alternative explanation is that the channel's biophysical properties are altered when removed from its native ionic environment or when it loses interactions with regulatory proteins. We will address this point in the Discussion.

> *(5) Could the authors use drugs against ASIC to specify which ASIC channels contribute to the pH response in the soma?*

As described in the manuscript, we performed experiments with ASIC antagonists, although we did not attempt to characterize the specific ASIC subtype mediating the somatic response. Based on the published literature, we used both psalmotoxin-1, which blocks ASIC1 channels, and APETx2, which blocks ASIC3 channels. The presence of ASIC1 in mouse CSFcNs has been demonstrated previously (Orts-Del'immagine et al. 2012; Orts-Del'Immagine et al. 2016), while ASIC3 has been identified in lamprey CSFcNs (Jalalvand et al. 2016). When applying an acidic solution to the soma, we recorded an inward current that was substantially blocked by psalmotoxin-1, although a small residual component persisted, consistent with the earlier findings of Orts-Del'Immagine et al. We did not attempt to block this remaining Psalmotoxin1-insensitive component.

> *(6) This is out of the scope of this study, but we did observe in fish a very rarely-opening channel in the PKD2L1KO mutant. I wonder if the authors have similar observations in the conditions where PKD2L1 is mainly in the closed state.*

We have never seen such kind of openings in our recordings (when the channel is closed or in the presence of dibucaine).

References

Bjugn, R, H K Haugland, et P R Flood. 1988. "Ultrastructure of the mouse spinal cord ependyma". Journal of Anatomy 160 (octobre): 117-25.

Bruni, J. E., et K. Reddy. 1987. "Ependyma of the Central Canal of the Rat Spinal Cord: A Light and Transmission Electron Microscopic Study". Journal of Anatomy 152 (juin): 55-70.

Delling, Markus, Paul G. DeCaen, Julia F. Doerner, Sebastien Febvay, et David E. Clapham. 2013. "Primary cilia are specialized calcium signaling organelles". Nature 504 (7479): 311-14 *https://doi.org/10.1038/nature12833*.

Hao, Jizhe, Jérôme Ruel, Bertrand Coste, Yann Roudaut, Marcel Crest, et Patrick Delmas. 2013. "Piezo-Electrically Driven Mechanical Stimulation of Sensory Neurons". In Ion Channels, édité par Nikita Gamper, vol. 998. Methods in Molecular Biology. Humana Press. *https://doi.org/10.1007/978-1-62703-351-0_12*.

Jalalvand, Elham, Brita Robertson, Hervé Tostivint, Peter Wallén, et Sten Grillner. 2016. “The Spinal Cord Has an Intrinsic System for the Control of pH”. Current Biology: CB 26 (10): 1346-51. *https://doi.org/10.1016/j.cub.2016.03.048*.

Nakamura, Yuka, Miyuki Kurabe, Mami Matsumoto, et al. 2023. “Cerebrospinal Fluid-Contacting Neuron Tracing Reveals Structural and Functional Connectivity for Locomotion in the Mouse Spinal Cord”. eLife 12 (février): e83108. *https://doi.org/10.7554/eLife.83108*.

Orts-Del’Immagine, Adeline, Riad Seddik, Fabien Tell, et al. 2016. “A Single Polycystic Kidney Disease 2-like 1 Channel Opening Acts as a Spike Generator in Cerebrospinal Fluid-Contacting Neurons of Adult Mouse Brainstem”. Neuropharmacology 101 (février): 549-65. *https://doi.org/10.1016/j.neuropharm.2015.07.030*.

Orts-Del’immagine, Adeline, Nicolas Wanaverbecq, Catherine Tardivel, Vanessa Tillement, Michel Dallaporta, et Jérôme Trouslard. 2012. “Properties of Subependymal Cerebrospinal Fluid Contacting Neurones in the Dorsal Vagal Complex of the Mouse Brainstem”. The Journal of Physiology 590 (16): 3719-41. *https://doi.org/10.1113/jphysiol.2012.227959*.

Prendergast, Andrew E., Kin Ki Jim, Hugo Marnas, et al. 2023. “CSF-Contacting Neurons Respond to Streptococcus Pneumoniae and Promote Host Survival during Central Nervous System Infection”. Current Biology 33 (5): 940-956.e10. *https://doi.org/10.1016/j.cub.2023.01.039*.

Trigo, Federico F., George Papageorgiou, John E. T. Corrie, et David Ogden. 2009. “Laser photolysis of DPNI-GABA, a tool for investigating the properties and distribution of GABA receptors and for silencing neurons in situ”. Journal of Neuroscience Methods 181 (2): 159-69. *https://doi.org/10.1016/j.jneumeth.2009.04.022*.

https://doi.org/10.7554/eLife.109372.1.sa0